CFD study of a NACA 63-415 aerofoil fitted with stall strips

Zahle, Frederik; Sørensen, Niels N.; Johansen, Jeppe

Publication date:
2002

Document Version
Publisher's PDF, also known as Version of record

Risø-R-1370(EN)

CFD Study of a NACA 63-415 Aerofoil Fitted with Stall Strips

Frederik Zahle, Niels N. Sørensen, Jeppe Johansen

Risø National Laboratory, Roskilde
September 2002

Abstract The present work describes a thorough investigation of 2D computations of the flow around a NACA 63-415 aerofoil fitted with stall strips (SS). A mesh study as well as a time step study is carried out and all computations are compared with experiments. Two different SS, 5mm and 7mm are investigated at several positions. Furthermore the influence of laminar to turbulent transition and the effect of a rounded SS were tested.

There is not sufficient agreement between the experimental results and the simulations to draw any conclusions of optimum position and geometry of the SS. The 7mm SS's placed at P00 and P-02 has the greatest effect on the max lift followed by SS P02. The 5mm SS's does, as in the experiment, not change the lift curve noticeably. Even though this investigation does not conclusively succeed in verifying the experimental results with CFD, many useful conclusions can be drawn from the results.

It is observed in the experiment that the vertical force fluctuates at higher angles of attack. This indicates that small bubbles are being shed off the profile causing the force to vary. This property is observed when transition is included in the model and also when the tip of the SS is rounded. From this result it could be concluded that the level of turbulence produced on the tip of the SS is very important for the development of the flow downstream. In the sharp tip calculations using fully turbulent computations, this is most likely too high, which resulted in the fine structures being damped out, with only one bubble appearing.

ISBN 87-550-3126-9
ISBN 87-550-3127-7 (Internet)
ISSN 0106-2840

Print: Pitney Bowes Management Services Denmark, 2002

Contents

1 Introduction 5

2 Mesh Study of a Clean NACA 63-415 Aerofoil 6

2.1 Mesh Type Investigation 6
2.2 Mesh Refinement Investigation 6

3 Stall Strips 8

3.1 Stall Strip Configuration 8
3.2 Numerical Study 9

4 Discussion 11

4.1 Sharp tip Stall Strips 11
4.2 Rounded Tip Stall Strips 14
4.3 Added Free-stream Turbulence 16

5 Conclusion 20

6 Results 22

6.1 Sharp Tip Stall Strips 22
6.2 Rounded Tip Stall Strips 42

Acknowledgements 48

References 48

Appendix 1 49

Appendix 2 51

1 Introduction

This report describes a two-dimensional CFD study done on the NACA 63-415 aerofoil fitted with stall strips (SS), and compares these results to the experimental results from the Velux Wind tunnel conducted by Fuglsang *et al*. [1].

The meshes were generated using the in-house mesh generator HypGrid2D [2], and the CFD calculations were done with the 2D Navier-Stokes flow solver EllipSys2D [3] [4] [5].

Stall Strips serve the purpose of controlling the stall characteristics of a wind turbine blade both with respect to power and loads. The aim is to achieve smooth post stall behaviour such that the undesirable stall induced vibrations are reduced, and at the same time minimising the drag penalty associated with the stall strip. It was hypothesised that placing the stall strip just below the leading edge as opposed to directly on the leading edge would reduce this drag penalty. However, in the tests it was found that placing stall strips in this position had very little benefits and for some cases did not improve the stall behaviour sufficiently.

Firstly a mesh study of a clean aerofoil and one fitted with stall strips will be carried such that a mesh independent solution can be presented. Secondly, the numerical consequences of placing such a bulky object on the tip of the aerofoil will be investigated.

Following this the report aims to verify the test results and to further investigate the flow characteristics of the aerofoil fitted with stall strips. It is important not only to identify the direct effects on the driving forces and the loads, but also to understand the physical behaviour of the flow in order to improve the efficiency of the stall strip in further development.

2 Mesh Study of a Clean NACA 63-415 Aerofoil

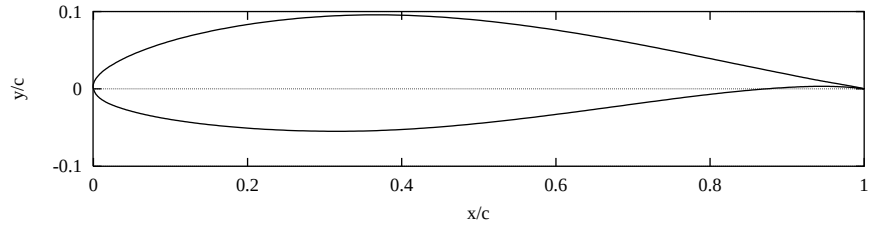

Figure 1: The NACA 63-415 aerofoil

2.1 Mesh Type Investigation

A 2D steady state mesh study was conducted on the NACA 63-415 aerofoil, where a comparison between a C-mesh and an O-mesh was made. The three meshes that were investigated had resolutions 384x64, 384x128 and 768x128. It was found that the O-meshes all converged faster than the corresponding C-meshes.

In this study it is particularly important that the flow in the wake is captured accurately since the stalling behaviour of the aerofoil is of most interest. It was decided that a C-mesh would be used in the further analysis, since this type of mesh could be expected to predict the flow in the wake region more accurately, as discussed in [6].

2.2 Mesh Refinement Investigation

In order to decide which resolution should be used in the further analysis another mesh study was done for the C-mesh. As in the Velux experiments the Reynolds number was set at $1.6 \cdot 10^6$. The flow was taken to be fully turbulent and unsteady and a non-dimensional time step of 10^{-2} defined by $t^* = t \cdot u/c$ was used. The SUDS convective scheme was used along with the k-ω SST turbulence model. For high angles of attack the time progression of the vertical and horizontal forces was highly unsteady but periodic. The resultant forces were calculated as an average of the periodic forces as was appropriate for each incidence. Three meshes were investigated:

- Mesh A1: 64 cells in the normal direction to the aerofoil, 256 around the aerofoil, and 64 cells in the wake.
- Mesh A2: 128 cells in the normal direction, 256 cells along the aerofoil and 64 cells in the wake.
- Mesh A3: 128 cells in the normal direction, 512 cells along the aerofoil and 128 cells in the wake.

For all meshes the height of the cells along the surface of the aerofoil was $10^{-5}\times$chord length. The angle of the cells in the wake was set at 10° in order to capture the wake flow more accurately.

Figure 2 shows the lift curve for the NACA 63-415 aerofoil for the three meshes tested. The three meshes show good correlation for incidences up to 14 degrees, with only a slight alteration when increasing the number of cells in the

normal direction. At higher incidences the three curves separate slightly, and give different values for each incidence. At these high incidences it is very unlikely that the solution is accurate since the flow becomes highly unstable.

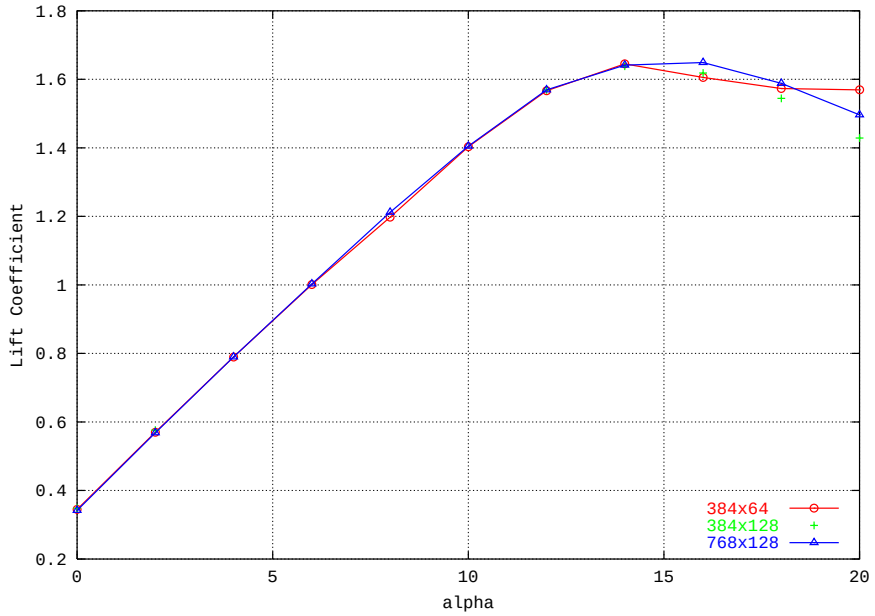

Figure 2: Lift vs. incidence for three different meshes

It could be argued that mesh A1 would be adequate for the investigation, since the solution only changes marginally when refining the mesh. However, due to the fact that stall strips will be placed on the aerofoil a higher resolution in the normal direction is desirable. The mesh A2 was therefore chosen for the SS investigation. A copy of the mesh generator input files for the final mesh can be found in Appendix 1.

3 Stall Strips

3.1 Stall Strip Configuration

The meshes for the aerofoil fitted with SS's were generated for the cases described in [1]. The chord length of the profile tested in [1] was 0.6 m. See Table 1 and Table 2 below for a summary of these configurations.

Table 1: Positions of the three 7mm SS on the aerofoil

Denotation	Stagnation Point at AOA [°]	Chord-wise position [%]	Non-dimensional side length [l/c]
P-02	-2	0.23	0.011667
P00	0	0	0.011667
P02	2	0.23	0.011667

Table 2: Positions of the three 5mm SS on the aerofoil

Denotation	Stagnation Point at AOA [°]	Chord-wise position [%]	Non-dimensional side length [l/c]
P06	6	1.02	0.008333
P10	10	2.57	0.008333
P14	14	4.07	0.008333

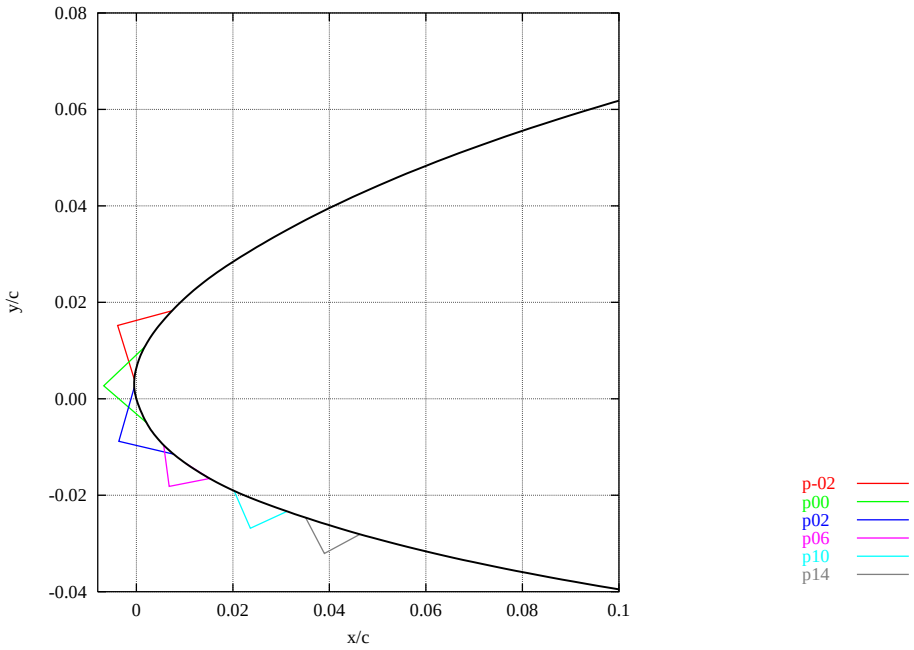

Figure 3: NACA 63-415 aerofoil with positions of the six SS's.

As described in [1] the SS's were triangular with internal angles of 45-45-90. The geometry of the 5mm SS's was modelled such that the height of the triangle protruding from the surface was exactly 5cos(45), whereas the 7mm SS was

done such that the sides were exactly 7mm. This is due to the fact that the 7mm SS had a curved inner surface in order for it to lie flush on the curved surface of the l.e. See Figure 3 for a plot of the aerofoil fitted with SS's.

3.2 Numerical Study

Mesh Refinement Investigation

This mesh study was done with the same time step and convective scheme, as well as with fully turbulent computations, as described in Section 2.2. The initial mesh contained 320 cell around the aerofoil, 128 in the normal direction and 64 in the wake. 40 cells were placed on the SS. This mesh is denoted M1.

Two other types of meshes were generated to investigate the importance of mesh density on the SS and l.e. Since the tip of the SS was modelled as an infinitely sharp edge this might cause some unnatural effects to occur here. Therefore, a high density of cells could help to reduce this error.

Mesh M2 was the same as M1 with an extra block of 64 cells added on the SS, thus resulting in 104 cells on the SS, with a total of 384 cells on the aerofoil surface. Mesh M3 was generated from M2 with another block of 128 cells added to the top surface, thus containing 512 cells around the aerofoil.

For mesh M1 the effect of SS's was only significant for P00 and P-02 where Cl_{max} was reduced considerably. Comparing these results to the experiment it would also be expected that a similar change would occur for P02. However this was not evident in the results obtained.

Increasing the number of cells on the SS altered the results considerably for all 7mm SS's, indicating that the previous mesh was far too coarse around and on the SS.

With mesh M3 there was no significant change in lift and drag compared to M2, hence mesh M3 was not used any further.

Refer to Appendix 1 for mesh input files.

Time step Investigation

It was speculated that a time step of 10^{-2} was too large to resolve the flow sufficiently at the SS tip. Especially the fine structures expected to occur on the upper side of the SS would need small time steps to be captured. from these considerations: the time taken for a particle to pass the SS $\cong$ 0.03, which means that with a time step = 0.02, the particle passes the SS in 1.5 time steps. Time steps of 10^{-3} and 10^{-4} were therefore tested on mesh M2.

Reducing the time step from 10^{-2} to 10^{-3} no significant changes were observed in the solutions. The same was the case for a time step of 10^{-4}. Therefore, a time step of 10^{-2} was chosen for all further calculations.

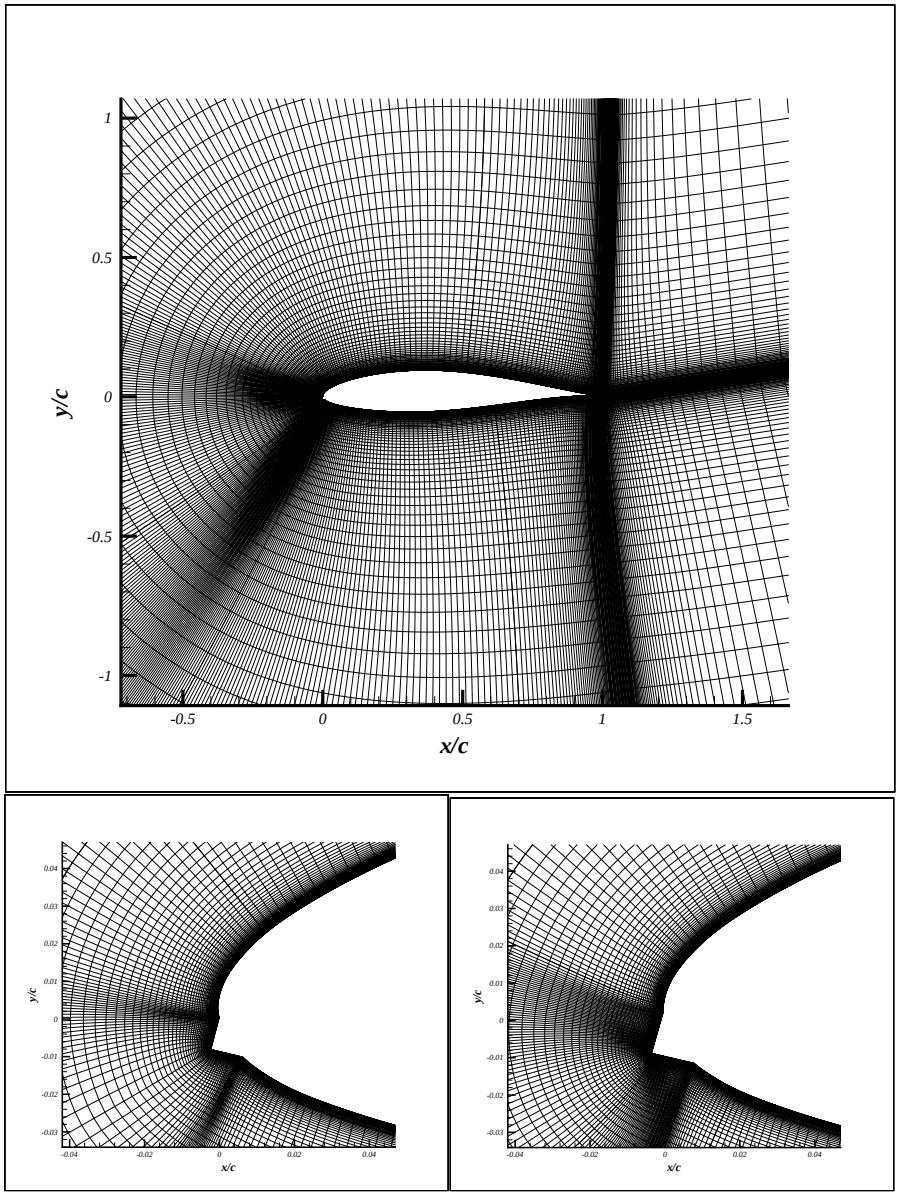

Figure 4: Above: Mesh M2, below: details of meshes M1 (left) and M2 (right)

4 Discussion

For results refer to Section 6. The Section is divided into three parts containing the results from the sharp tip calculations with fully turbulent computations, the sharp tip calculations using transitional computations, and the rounded tip calculations with fully turbulent computations and transitional computations presented together.

4.1 Sharp tip Stall Strips

Fully Turbulent Computations

The calculations were all done with unsteady computations, using mesh M2 (see Figure 4) with a time step of 10^{-2}. Throughout the simulations the SUDS convective scheme and the k - ω SST turbulence model by Menter were used.

Comparing the EllipSys2D lift curves of the clean NACA 63-415 aerofoil with the experiment, there was a pronounced difference not only in C_{lmax}, but also the lift curve slope (see Figure 16). This phenomenon is consistent with calculations done for other similar aerofoils, and is largely attributed to the free-stream turbulence level in the Velux wind tunnel. The effect of this will be discussed in more detail later in this section. As a result of the difference in C_{lmax} it was expected that this difference would carry on throughout the calculations, so it seemed more consistent to use ΔC_{lmax} as a measure of the effect of the SS's.

The Velux experiments by Fuglsang *et al.* [1], found that there was a pronounced effect of the three 7mm SS's positioned at P-02, P00 and P02 and next to no effect of the P06, P10 and P14 SS's. In the experiment SS P-02 had the greatest effect, where the two others at P00 and P02 had slightly higher C_{lmax}. The spread of the max lift coefficient of the three SS's was $\Delta C_{lmax} = 0.02$.

There was a varying degree of agreement between the experiment and the calculations. As shown in Figure 12 and Figure 13 the calculations showed the same trend as the experiment with the 5mm SS's causing almost no reduction in the lift peak and the 7mm SS's having increasing effect with P-02 giving the highest reduction in max lift. There was, however, a significant difference in the magnitude of the lift coefficients of the three 7mm SS's in the calculations and experiment. See Table 3 *and*

Table 4 below for a summary of the results.

Table 3: Summary of results for the sharp tip SS's assuming fully turbulent flow.

	Experiment		***EllipSys2D***			
SS	C_{lmax}	ΔC_{lmax}	C_{lmax}	ΔC_{lmax}	***Difference in C_l (%)***	***Difference in ΔC_{lmax}***
Clean	1.3319	-	1.5661	-	17.6	
P-02	0.9965	-0.3354	0.9412	-0.6250	-5.6	0.2896
P00	1.0482	-0.2837	1.0550	-0.5111	0.65	0.2274
P02	1.0296	-0.3023	1.3704	-0.1957	33.1	-0.1066
P06	1.25	-0.0819	1.5279	-0.0383	22.2	-0.0436
P10	1.3021	-0.0298	1.5585	-0.0077	19.7	-0.0221
P14	1.3121	-0.0198	1.5683	0.0022	19.5	-0.0220

Table 4: Summary of results for the sharp tip SS's assuming fully turbulent flow for $\alpha = 10°$.

	Experiment		***EllipSys2D***			
SS	C_d	ΔC_d	C_d	ΔC_d	***Difference in C_d (%)***	***Difference in ΔC_d***
Clean	0.0218	-	0.0368	-	-11.3	
P-02	0.0684	0.0466	0.0467	-0.0099	17.3	0.0565
P00	0.0624	0.0406	0.0288	0.0079	-20.6	0.0327
P02	0.0328	0.0110	0.0374	-0.0006	-23.9	0.0116
P06	0.0297	0.0079	0.0213	0.0155	-28.4	-0.0076
P10	0.0203	-0.0015	0.0208	0.0160	2.47	-0.0175
P14	0.0202	-0.0016	0.0208	0.0159	3.18	-0.0175

With SS P02 fitted, C_{lmax} was considerably higher than for the two other 7mm SS's, and higher than what found in the experiment (Figure 20 to Figure 23). SS's P00 and P-02 behaved differently from P02, and the change in max lift was much higher than expected comparing to the experiment (Figure 16 to Figure 19, Figure 24 to Figure 27). Tecplot pressure contour plots were produced for the three configurations, which in conjunction with the pressure distribution plots helped to explain the pronounced differences (Figure 6 and Figure 7). The behaviour of the l.e. separation bubble caused by the disturbance in the flow from the SS was clearly different. SS P02 only caused a small separation where the flow reattached before it reached the top surface. A much larger separation bubble was produced for SS's P00 and P-02, which expanded along the top surface before bursting and causing complete stall.

As in the experiment the 5mm SS's did not have much effect (Figure 28 to Figure 39). SS P06 had the greatest impact on C_{lmax} and the two others resulted in virtually no change. This was due to the fact that the disturbance caused by the SS was damped out by the acceleration of the flow around the l.e., thus not causing a l.e. separation bubble to occur.

In conjunction with the experimental results it should be emphasised that due to the nature of the Velux wind tunnel there is a high amount of free-stream turbulence estimated at about 1% (a detailed study of the tunnel can be found in [7]). This reduces the max lift of the clean aerofoil, and comparing the results to those from Abbot and van Doenhoff [8] there is a significant difference in max

lift. It should be noted that the results from [8] are in much better agreement with the EllipSys2D calculations. This is discussed in more detail in [9]

As discussed above the mechanism governing the effect of the SS is largely dependent on the formation of a l.e. separation bubble. Introducing free-stream turbulence most likely alters the formation of such a bubble by increasing the mixing of the fluid around the SS. This could explain why there was no significant difference when placing the SS just above and below the l.e. in the experiment, whereas in the simulations this was very pronounced.

The time progression of the vertical force for SS P02 at $\alpha = 20°$ was highly unsteady varying from 0.7 to 2.3. The calculated lift coefficient was found on average to be 1.82. A contour plot of the flow reveals that a large separation bubble was produced at the l.e., which travelled downstream producing the extreme lift coefficients. A closer look at the pressure and viscosity variation around the t.e. showed that there were large discontinuities across the block boundaries in the wake and in the dense region above the t.e., possibly entrapping the flow in this region. A pressure contour plot of this is shown in Figure 11. This phenomenon occurs in the solution because the stiffness of the system of equations used in the code is high where the aspect ratio of the cells is high as seen in the wake. This inhibits the smoothing of high pressure gradients. Since this might have been the cause of the large fluctuations in lift force, various meshes were produced with higher volume blending and wake configurations. The number of sub iterations was also increased from three to nine. This however, did not eliminate the large force fluctuations and pressure discontinuities. The data point containing this numerical error was therefore omitted from the results.

This phenomenon was not observed for other incidences or configurations of the sharp tip SS's, but it is likely that calculations at higher incidences would reveal the same behaviour.

Another source of error in the numerical results could be the dimesionless normal distance, y+. This value should not exceed a value of 2 at any point in the flow. It was speculated that due to the high gradient at the tip of the SS this might occur. It was found, however, that the maximum was 1.8, which was acceptable. A definition of y+ can be found in Appendix 2.

Transitional Computations

Since the fully turbulent calculations did not yield satisfactory results a set of polars were produced for P-02, P00, and P02 using the Michel transition model. This altered the results somewhat, increasing the max lift for P00 and P-02, but also increasing the max lift for P02 slightly. The max lift for the clean aerofoil was reduced significantly.

The Section Transitional Computations on Page 36 contains the plots produced for the three configurations and Table 5 and Table 6 summarise the results obtained.

Table 5: Summary of results for the sharp tip SS's using transitional computations.

	Experiment		***EllipSys2D***			
SS	C_{lmax}	ΔC_{lmax}	C_{lmax}	ΔC_{lmax}	***Difference in*** C_d ***(%)***	***Difference in*** ΔC_{lmax}
Clean	1.3319	-	1.4684	-	10.2	
P-02	0.9965	-0.3354	0.9440	-0.5244	-5.27	0.1890
P00	1.0482	-0.2837	1.0918	-0.3766	4.16	0.0929
P02	1.0296	-0.3023	1.3820	-0.0863	34.2	-0.2160

Table 6: Summary of results for the sharp tip SS's using transitional computations for $\alpha = 10°$.

	Experiment		***EllipSys2D***			
SS	C_d	ΔC_d	C_d	ΔC_d	***Difference in C_d (%)***	***Difference in ΔC_d***
Clean	0.0218	-	0.0182	-	-16.5	
P-02	0.0684	0.0466	0.0781	0.0599	14.2	-0.0133
P00	0.0624	0.0406	0.0468	0.0286	-25.0	0.0120
P02	0.0328	0.0110	0.0264	0.0081	-19.7	0.0029

The flow around the SS's behaved significantly different when transition effects were taken into account. It produced a more unsteady behaviour with several small bubbles forming on the SS tip (see Figure 8 for a contour plot). The reason for this was that the transition to turbulent flow did not occur until just downstream of the SS tip, thus reducing the turbulence production, allowing the smaller structures in the flow to remain intact.

However, to conclude that this is a valid solution simply due to the fact that it lies closer to the experimental results is not easy, because the experimental results were done under very different conditions from the conditions set in EllipSys2D. What can be deducted from these results is that the high levels of turbulence produced on the sharp tip SS's could cause the flow not to be captured properly, thus reducing this would yield a more physical solution.

As expected the SS triggered earlier transition than the clean aerofoil. Also, the transition point was now fixed at one point, which is an important factor when attempting to reduce the induced vibrations in the turbine blades.

The same phenomenon of pressure and viscosity discontinuities as discussed in Section 4.1 was observed for $\alpha = 18°$ for SS P00. Although not as extreme, it was observable in a contour plot. This phenomenon could easily have gone unnoticed, because the change in lift was small and could have been mistaken for a natural phenomenon, which was observed in the experiments. Similarly the data point at $\alpha = 20°$ for the clean lift curve had to be omitted. In the time frame of the project it was not possible to produce a mesh, which was free of this error.

4.2 Rounded Tip Stall Strips

Fully Turbulent Computations

In the experiment it was observed that the vertical force fluctuated with time, which indicated that small bubbles were thrown off the SS, travelling downstream. For the sharp tip SS calculations this phenomenon was not present for the fully turbulent flow. As shown in Figure 6 the separation bubble formed is a stationary re-circulating bubble, which is held in place by the high levels of turbulence produced on the SS tip. It was shown with the transition calculations that in fact a reduced amount of turbulence allowed for a more natural development of the flow downstream of the SS. A rounded tip could possibly reduce this production, even though the geometry would not strictly correspond to the experiment.

The very high pressure gradients on the tip of the SS, present in the calculations and not in the experiment (Figure 14 and Figure 15), indicated that the resolution at this point was not high enough. In order to capture the true nature

of the flow in this region the mesh would have to be infinitely dense. Therefore it was speculated that adding curvature to the SS tip would enable a more detailed representation of the flow, without having to increase the mesh density significantly.
Two types of meshes were tested for the rounded tip SS's. The first one (see

Figure 5) had 104 cells on the SS, the same as mesh M2 described in Section 3.2. The second mesh had an increased amount of cells on the SS and top surface, 168 and 256 respectively. The time step, convective scheme and the flow was taken to be fully turbulent. A smaller time step of 10^{-3} was also tested on the new geometry. No significant alteration of the results was observed with the finer mesh or with a smaller time step; hence the initial mesh was used for all calculations.

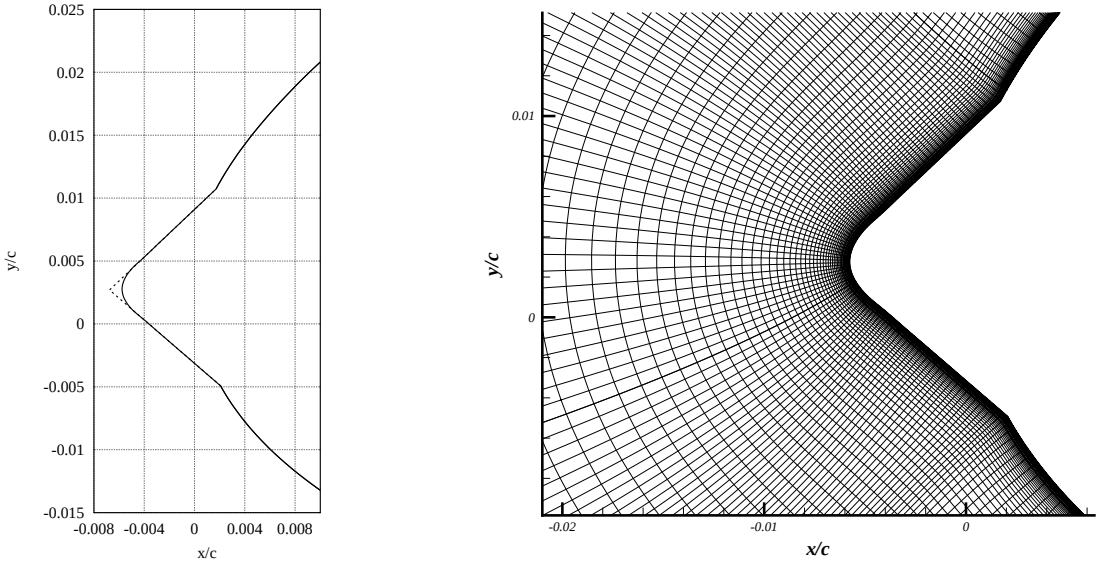

Figure 5: Modified SS with rounded tip

Table 7: Summary of results for the rounded tip SS's.

	Experiment		***EllipSys2D***			
SS	C_{lmax}	ΔC_{lmax}	C_{lmax}	ΔC_{lmax}	***Difference in C_d (%)***	***Difference in ΔC_{lmax}***
Clean	1.3319	-	1.5661	-	17.58639	
P-02	0.9965	-0.3354	0.9690	-0.5972	-2.76203	0.2618
P00	1.0482	-0.2837	1.1275	-0.4387	7.561251	0.1550
P02	1.0296	-0.3023	1.3925	-0.1736	35.25025	-0.1287

Table 8: Summary of results for the rounded tip SS's for $\alpha = 10°$.

	Experiment		***EllipSys2D***			
SS	C_d	ΔC_d	C_d	ΔC_d	***Difference in C_d***	***Difference in ΔC_d***
Clean	0.0218	-	0.0193	-	-11.2727	
P-02	0.0684	0.0466	0.0671	0.0478	-1.89071	-0.0012
P00	0.0624	0.0406	0.0409	0.0216	-34.3814	0.0190
P02	0.0328	0.0110	0.0238	0.0045	-27.4041	0.0065

As shown is Section 6.2 the modification increased the max lift for all the SS tested, most significantly for SS P00 (Figure 52) and P-02 (Figure 60). As speculated new structures of small shedded bubbles appeared downstream of the SS tip, causing the vertical force to fluctuate similar to the results with the transitional computations. A pressure contour plot of this is shown in Figure 9.

There was also a significant increase in lift coefficient in the post stall region for SS P-02 of 0.17 at $\alpha = 12°$.

The lift curve for P00 had a different shape in the post stall region, where between $\alpha = 14°$ and $\alpha = 16°$ the curve flattened out. A contour plot of this showed that the same numerical phenomenon occurred as was observed for the sharp tip SS P02 and P00 (transition) as discussed in Section 4.1 and 4.2. The data point SS P00, $\alpha = 16°$ had to be omitted from the results.

Transitional Computations

Calculations were also done with transition for the curved SS's (Figure 52 to Figure 63). The lift coefficient was increased for more or less all incidences. The behaviour of the SS's did not, however, resemble that found in the experiments any more than with the fully turbulent computations. The lift curve was merely shifted upwards for all SS's, with the same qualitative behaviour.

4.3 Added Free-stream Turbulence

Even though the solution was improved by rounding the tip of the SS, it still remained that the qualitative behaviour of the SS's was considerably different in the experiment.

An attempt was therefore made to simulate the free-stream turbulence that was present in the Velux tunnel experiments, which was speculated to cause the large difference in results. By adding a source of turbulence just upstream of the SS the level of turbulence in the flow approaching the SS was increased. The amount of turbulence added was arbitrary, so various intensities, positions and thickness of the source layer were tested.

Figure 10 shows a viscosity contour plot of the rounded P00 SS at $\alpha = 10°$. The addition of turbulence increased the max lift coefficient by 0.026 for this particular test, which was much less than needed. SS P02 was also tested, and the lift coefficient was reduced by 0.01.

The contour plot of SS P00 revealed that the flow changed in two significant ways due to the addition of this turbulence. Firstly, the l.e. separation bubble was reduced in size by 28%, and secondly, the separation point at the trailing edge had moved backward by 16%. At post stall angles of attack the flow remained attached for much longer, continuously increasing the lift coefficients. At higher intensities of added turbulence the flow barely separated, making the above effect even stronger.

It was therefore concluded that this simulation did not yield physically viable results and was therefore not investigated any further.

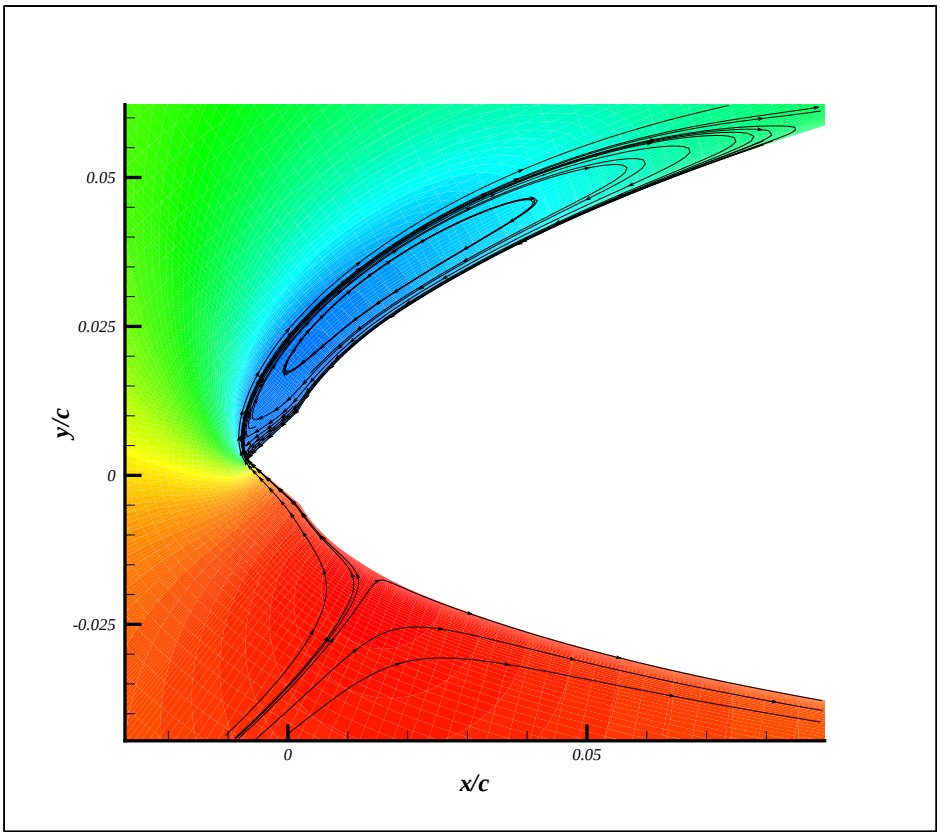

Figure 6: Pressure contour plot of flow with stream traces for 7mm, 0 deg SS, α = 12°. Calculations done using fully turbulent computations.

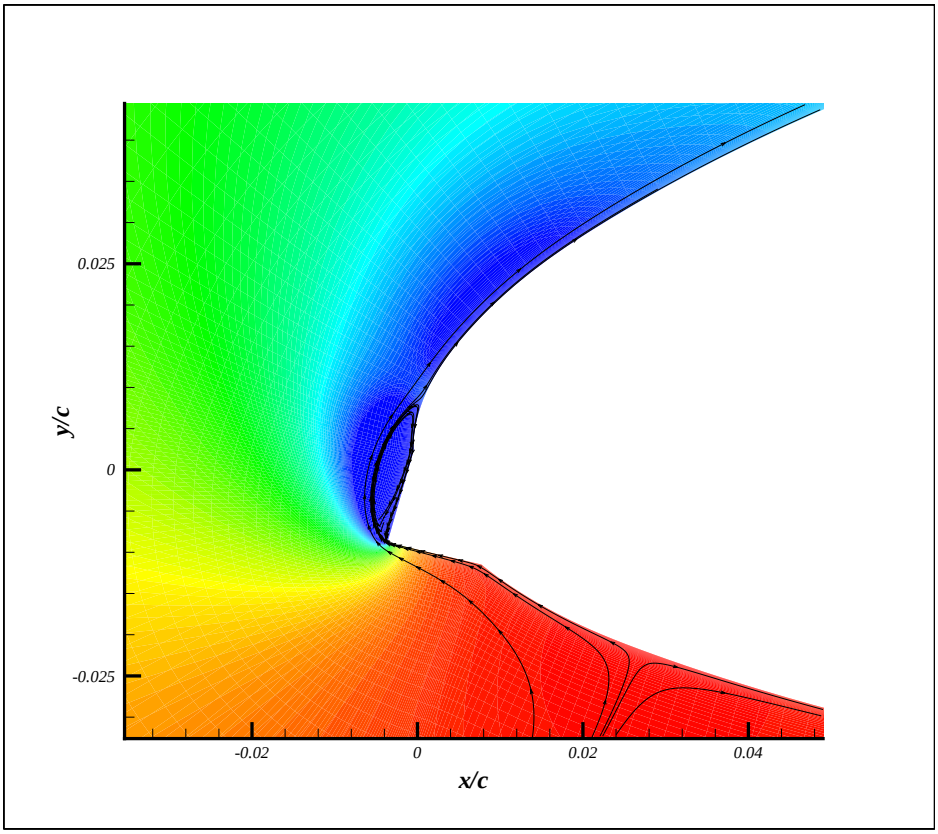

Figure 7: Pressure contour plot of flow with stream traces for 7mm, 2 deg SS, α = 12°. Calculations done using fully turbulent computations

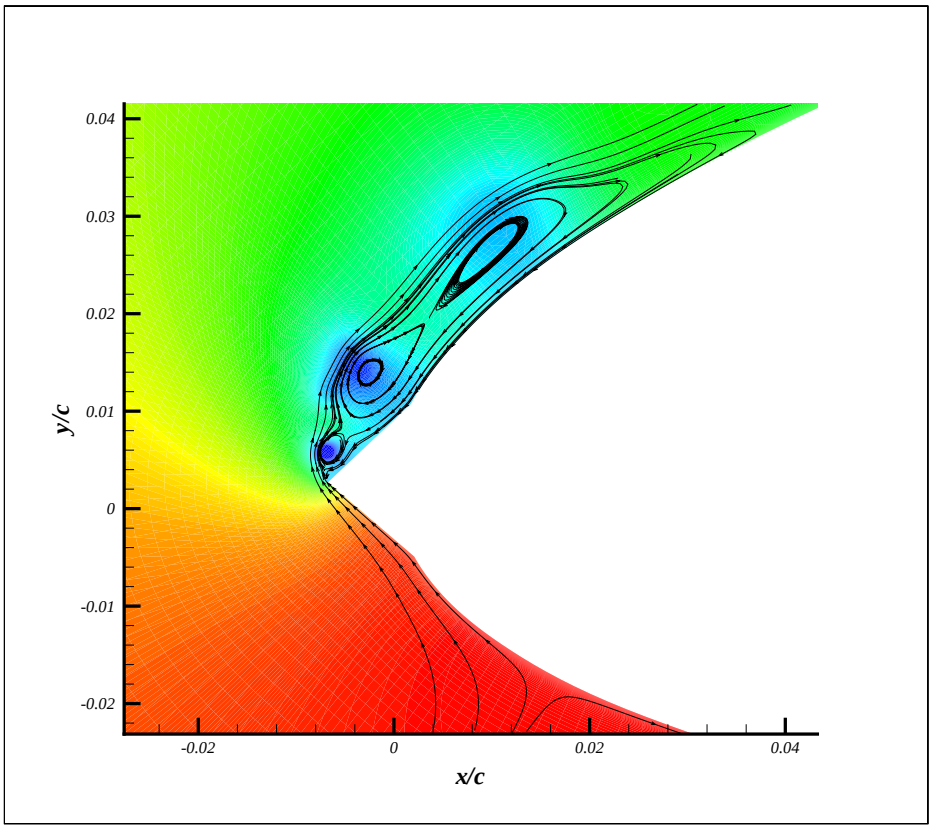

Figure 8: Pressure contour plot of 7mm, 0 deg SS, α=12°. Calculations done using transitional computations.

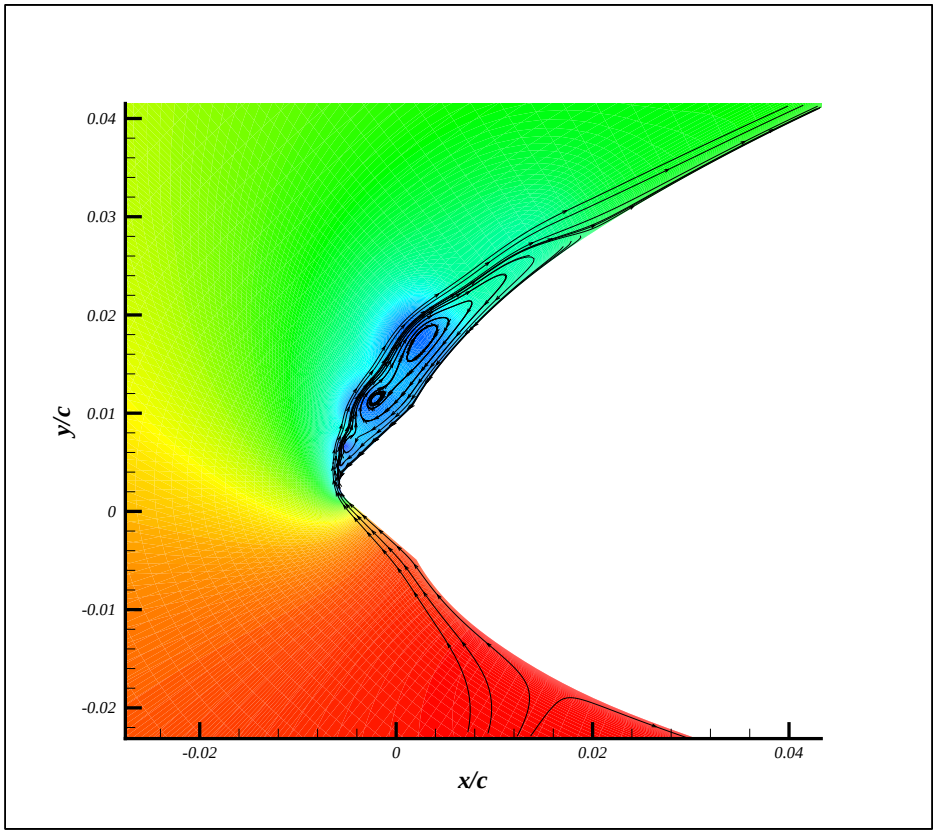

Figure 9: Pressure contour plot of flow with stream traces for 7mm, 0 deg rounded tip SS, $\alpha = 10°$. Calculations done using fully turbulent computations.

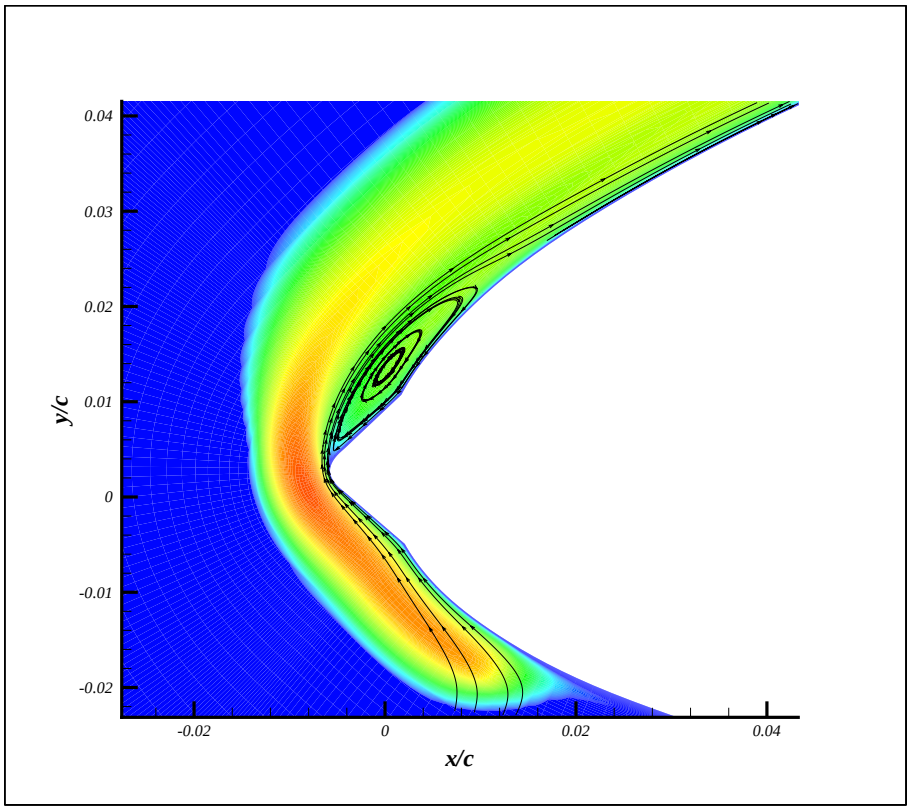

Figure 10: Viscosity contour plot of flow with stream traces for 7mm, 0 deg SS, $\alpha = 10°$, with added turbulence. Calculations are done using fully turbulent computations.

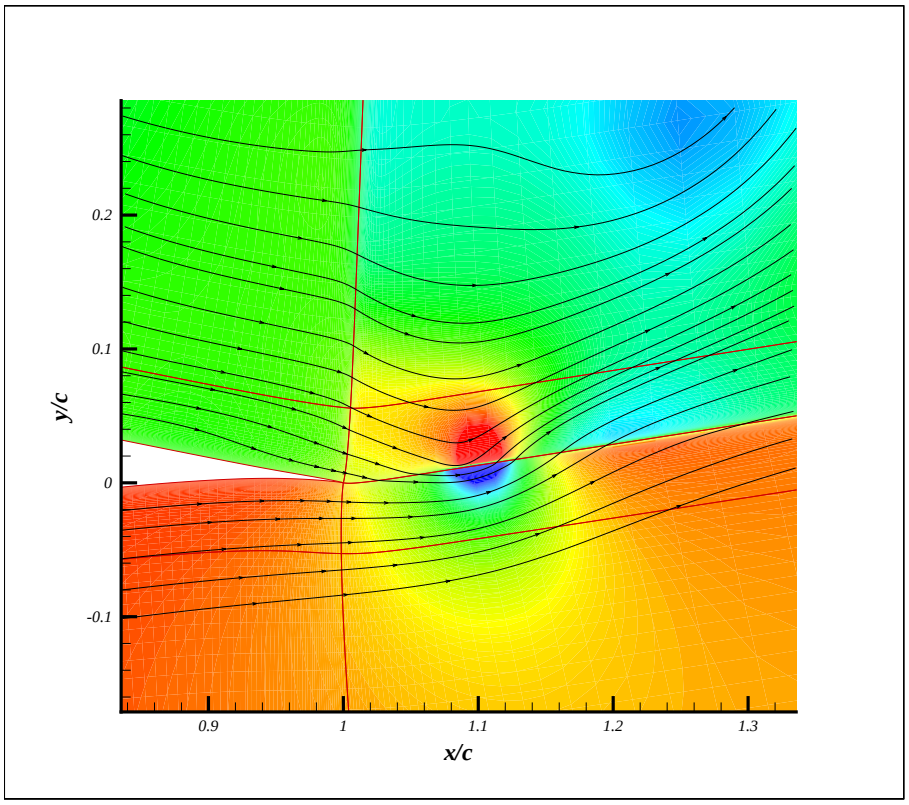

Figure 11: Pressure contour plot of flow with stream traces for 7mm, 2 deg SS, $\alpha = 20°$, showing the pressure discontinuities across the boundaries.

5 Conclusion

In this investigation a thorough 2D mesh study as well as a time step study of an aerofoil fitted with SS's was carried out. The mesh used had 384 cells around the aerofoil, 104 of which were concentrated on the SS. A non-dimensional time step of 10^{-2} was used throughout the investigation.

There was not sufficient agreement between the experimental results and the simulations to draw any conclusions of optimum position and geometry of the SS. The 7mm SS's placed at P00 and P-02 had the greatest effect on the max lift followed by SS P02. The 5mm SS's did, as in the experiment, not change the lift curve noticeably.

Even though this investigation did not conclusively succeed in verifying the experimental results with CFD, many useful conclusions can be drawn from the results.

The mechanisms governing the flow properties of an aerofoil fitted with SS's are very complex, because it mostly depends on the nature of the l.e. separation bubble occurring downstream of the SS. Separation is one of the most multifaceted mechanisms to model numerically, and it is therefore likely that the flow is not accurately modelled with the current code. Furthermore, separation is a highly three-dimensional phenomenon, so a 2D model is possibly not sufficient to understand the physics of SS's completely.

It was observed in the experiment that the vertical force fluctuated at higher angles of attack. This indicated that small bubbles were being shedded off the

profile causing the force to vary. This property was observed when transition was included in the model and also when the tip of the SS was rounded. From this result it could be concluded that the level of turbulence produced on the tip of the SS was very important for the development of the flow downstream. In the sharp tip calculations using fully turbulent computations, this was most likely too high, which resulted in the fine structures being damped out, with only one bubble appearing.

Four data points had to be omitted from the results, because there were errors in the numerical solutions produced. This was evident in the contour plots, where large discontinuities across the block boundaries in the wake were present. Attempts were made to generate new meshes where this phenomenon was not present, but the time frame of the project did not allow for this to be completed.

Further study of SS's could involve a more detailed analysis of the importance of the geometry of the SS. In this investigation the transition between the profile and SS was modelled as completely smooth. In the experiments it is likely that there was a step or gap between the two, possibly triggering earlier separation or turbulence.

To get a better understanding of the behaviour of SS's it is suggested that the SS's are modelled in three dimensions, such that the true behaviour of the l.e. stall can be investigated. For such an investigation it would be necessary to implement Detached Eddy Simulation, in order to get significantly different results from the 2D calculations. Furthermore, it was observed that when transition was taken into account, the flow significantly changed behaviour. The Michel transition model used is a fairly simple model, whereas a more detailed model might show that the transition effects observed are of bigger importance to the flow development.

6 Results

6.1 Sharp Tip Stall Strips

Fully Turbulent Computations

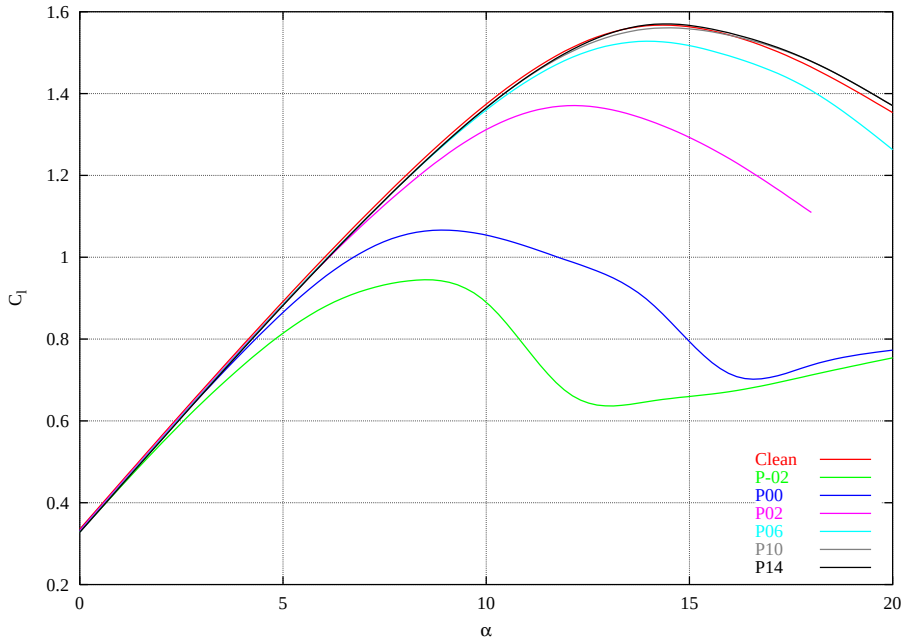

Figure 12: Lift curves for the six SS configurations and for the clean aerofoil

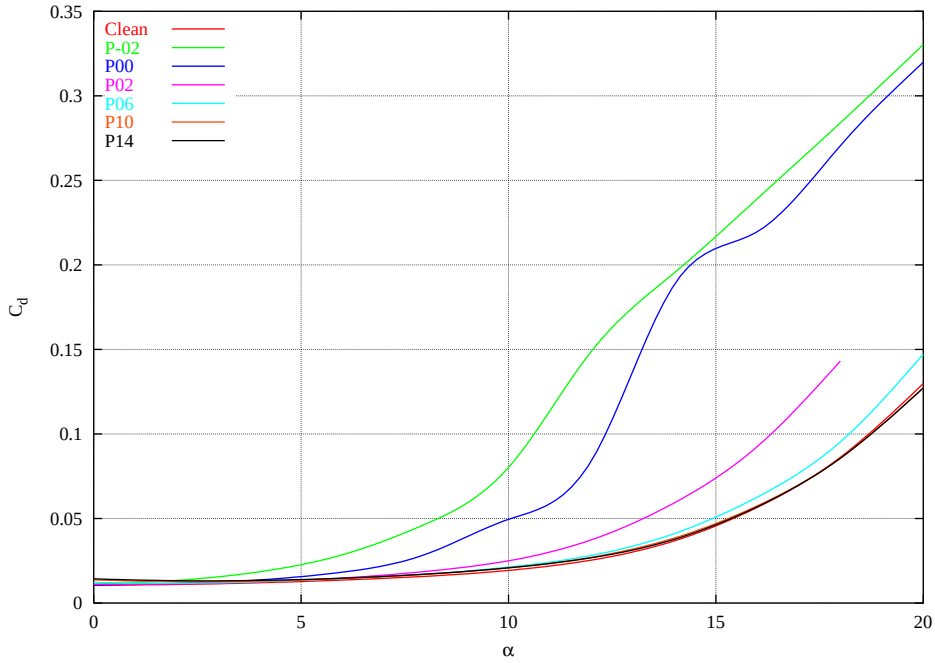

Figure 13: Drag curves for the six configurations and for the clean aerofoil

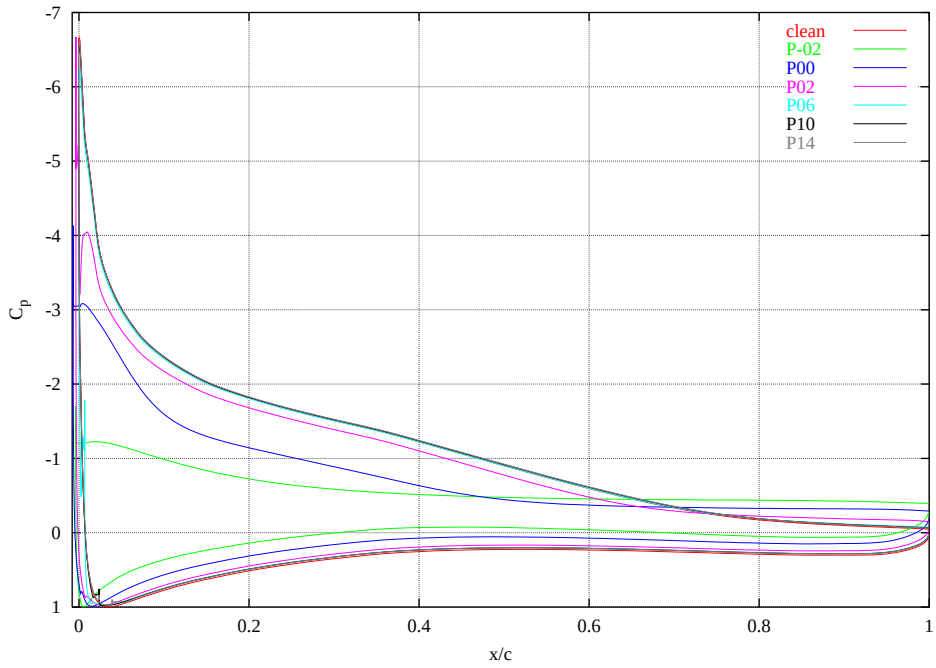

Figure 14: Pressure distributions for the six SS configurations and for the clean aerofoil, α=12°.

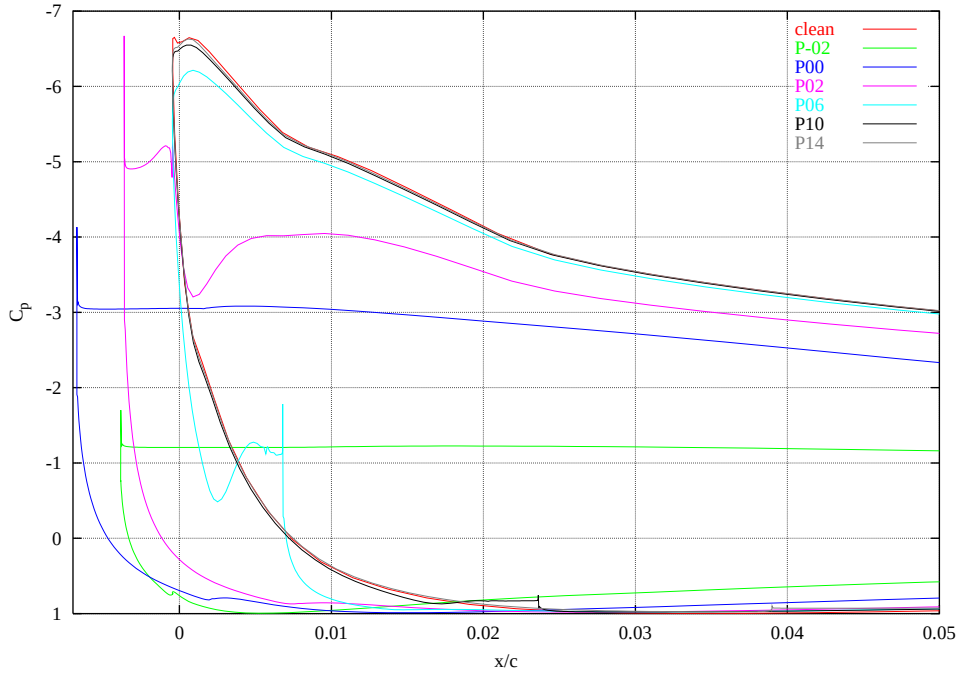

Figure 15: Detail of above plot.

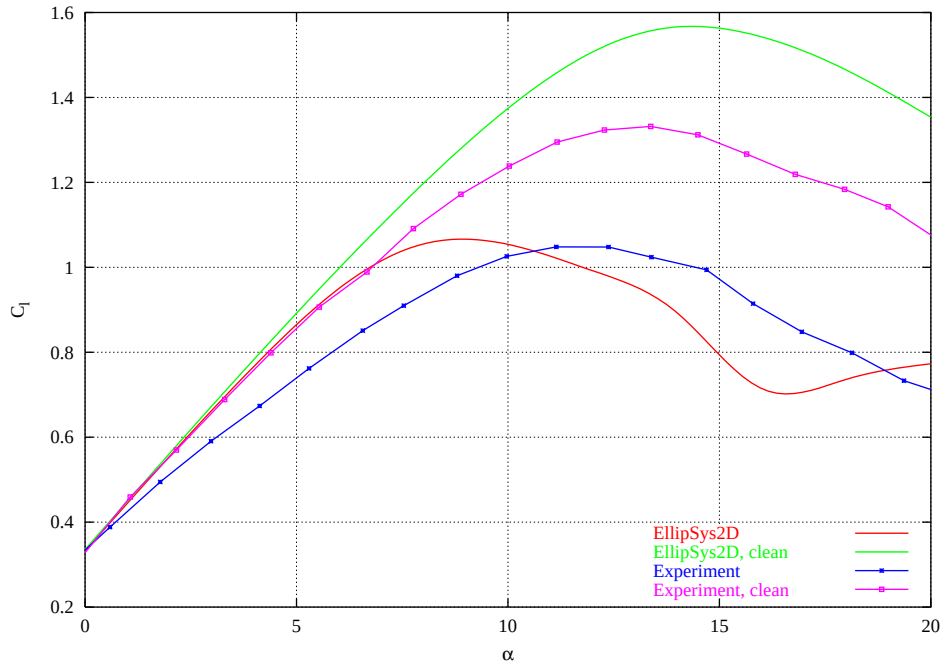

Figure 16: Experimental lift curve for the 7mm, 0 deg SS compared to Ellip-Sys2D calculation.

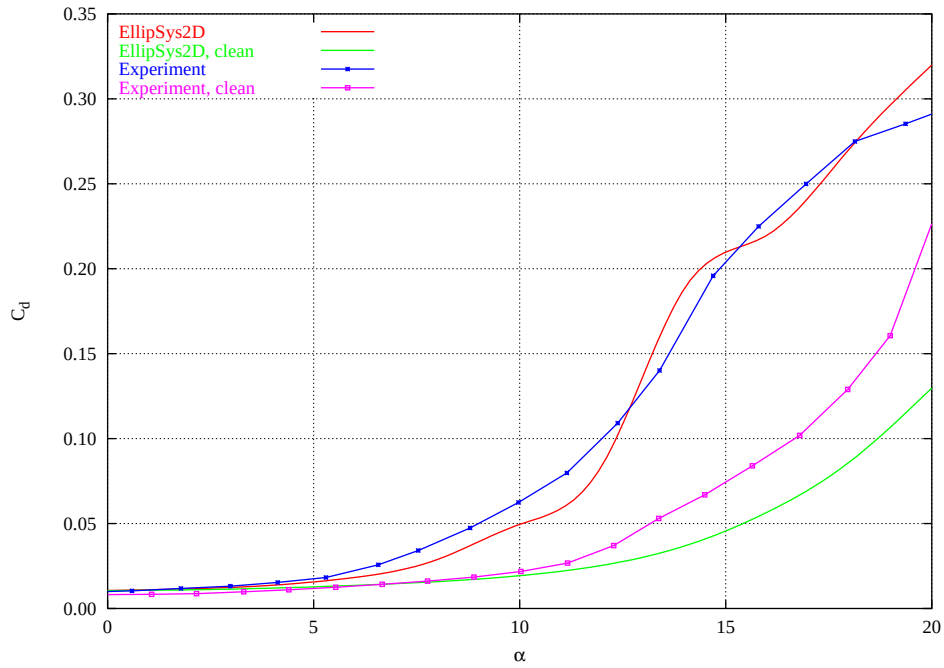

Figure 17: Experimental drag curve for the 7mm, 0 deg SS compared to Ellip-Sys2D calculations.

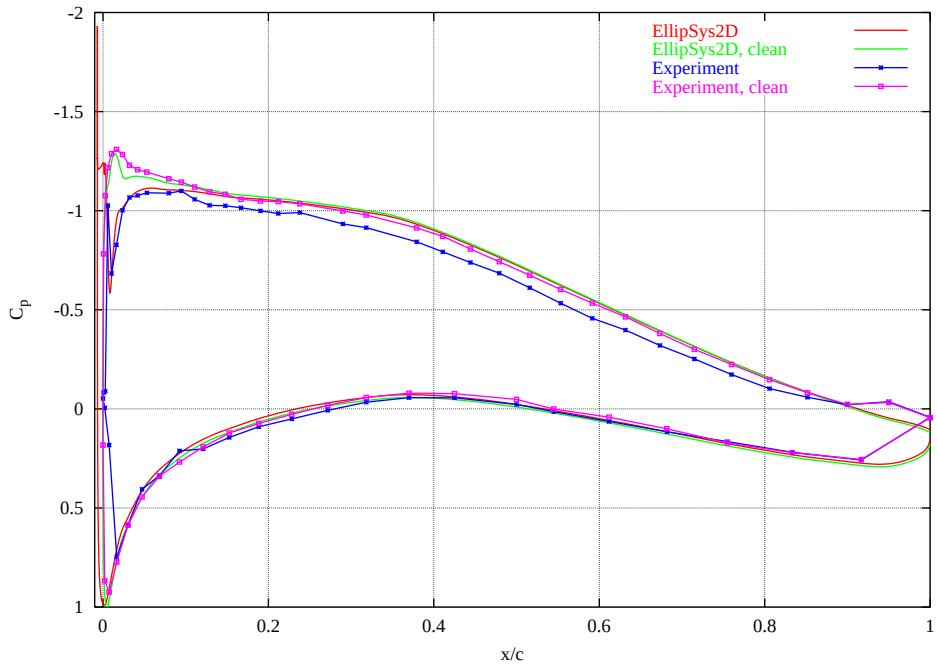

Figure 18: Experimental pressure distribution for the 7mm, 0 deg SS compared to EllipSys2D calculations, α=4°.

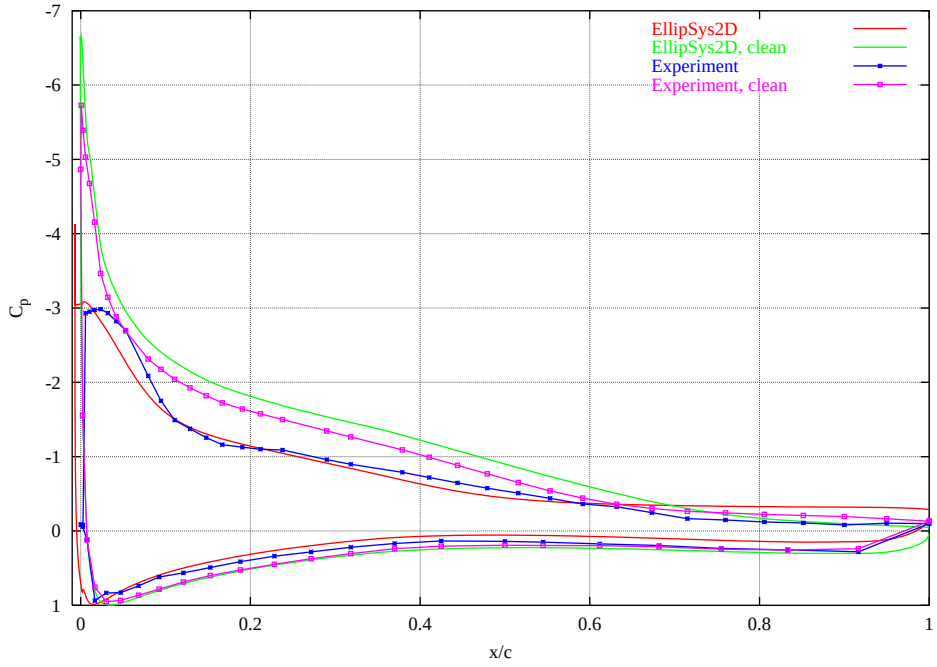

Figure 19: Experimental pressure distribution for the 7mm, 0 deg SS compared to EllipSys2D calculations, α=12°.

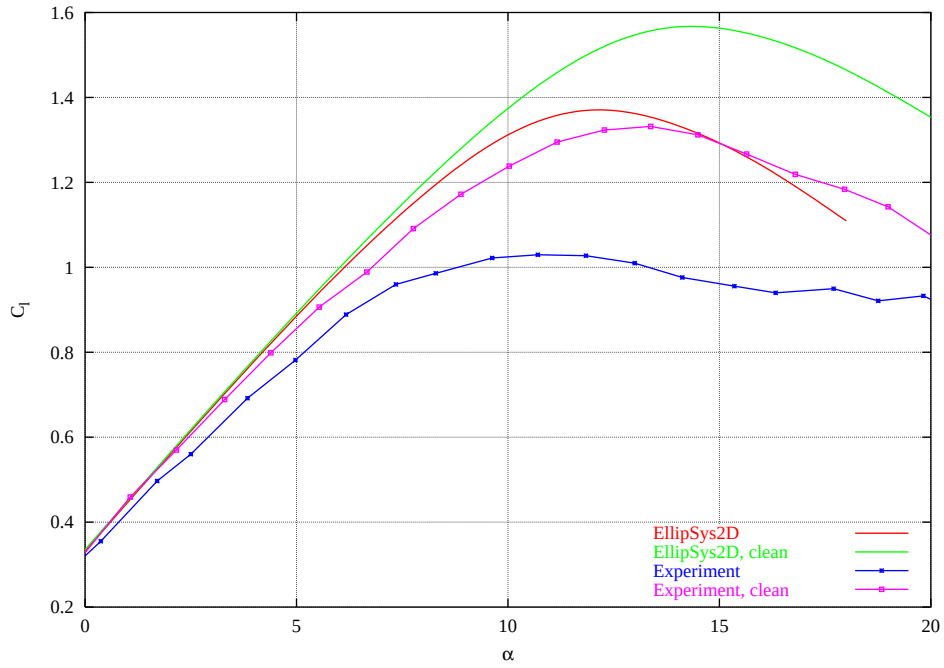

Figure 20: Experimental lift curve for the 7mm, 2 deg SS compared to Ellip-Sys2D calculations.

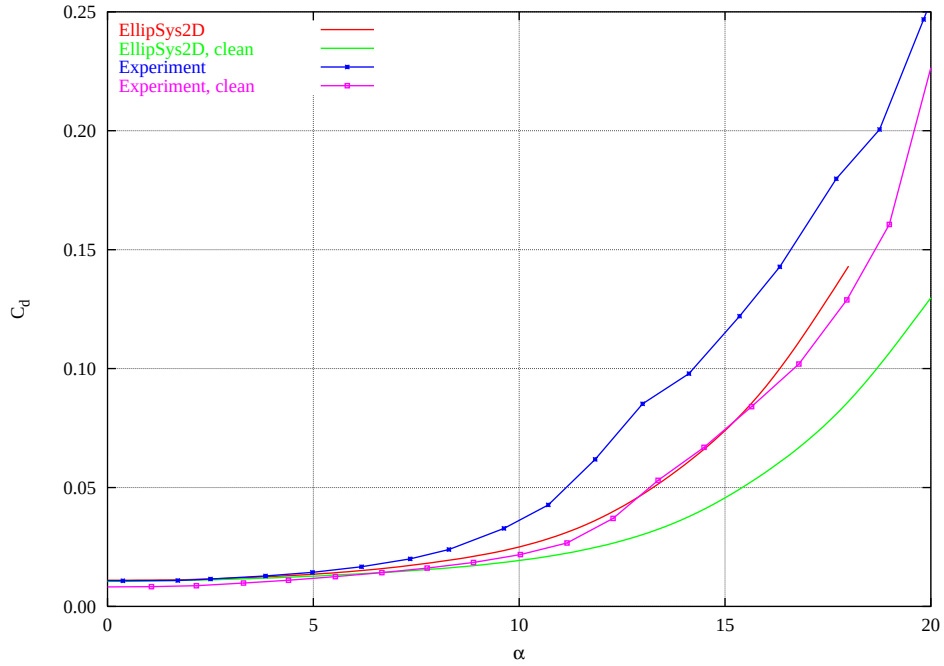

Figure 21: Experimental drag curve for the 7mm, 2 deg SS compared to Ellip-Sys2D calculations.

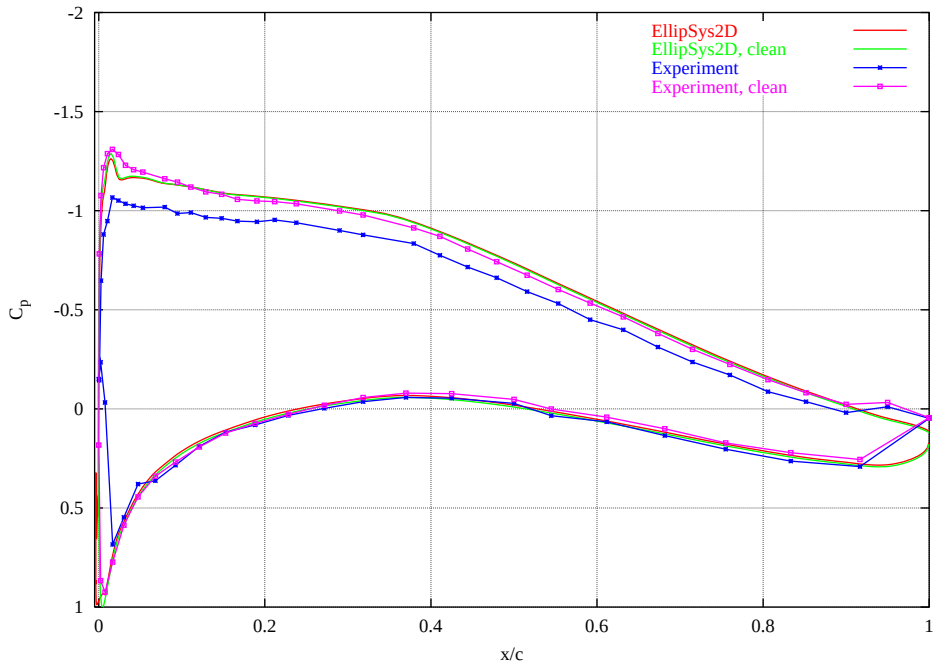

Figure 22: Experimental pressure distribution for the 7mm, 2 deg SS compared to EllipSys2D calculations α=4°.

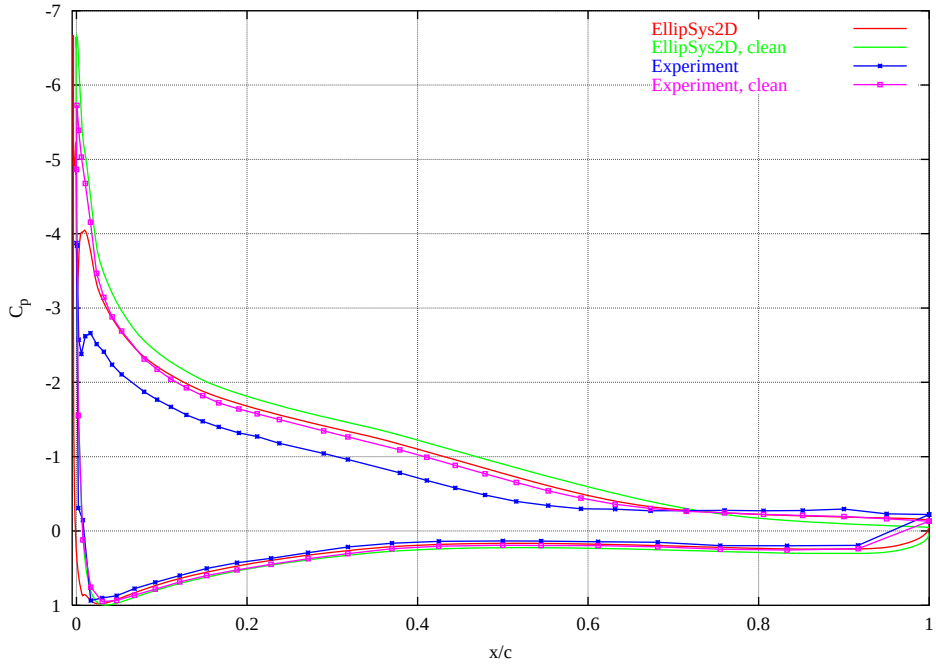

Figure 23: Experimental pressure distribution for the 7mm, 2 deg SS compared to EllipSys2D calculations α=12°.

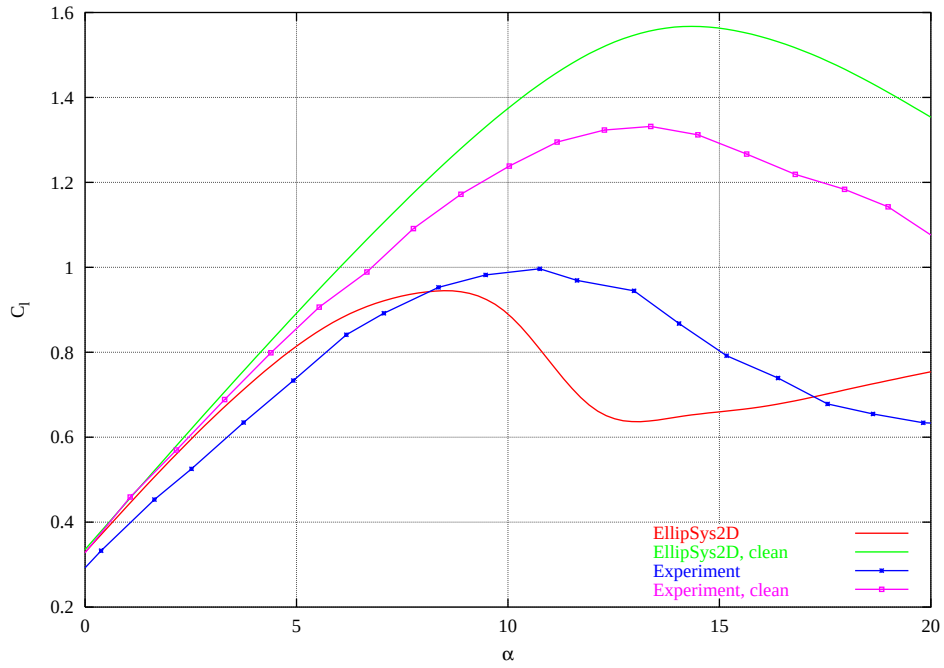

Figure 24: Experimental lift curve for the 7mm, -2 deg SS compared to EllipSys2D calculations.

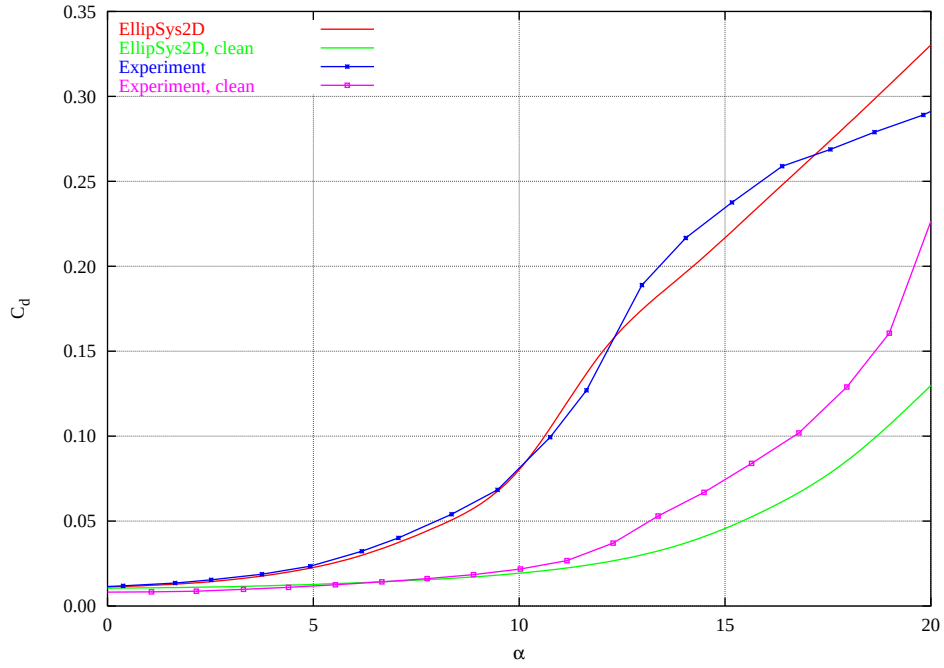

Figure 25: Experimental drag curve for the 7mm, -2 deg SS compared to EllipSys2D calculations

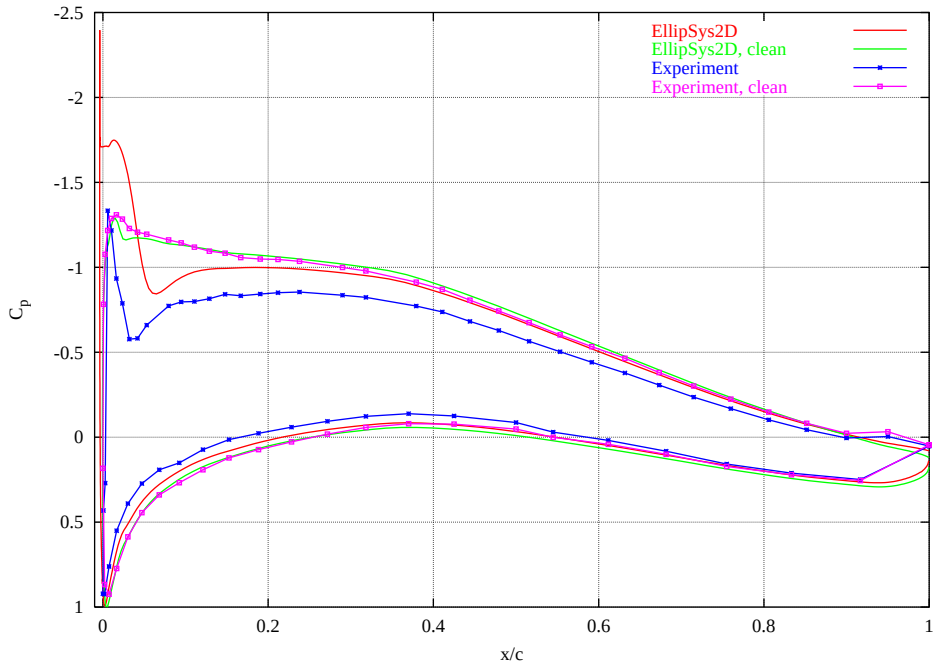

Figure 26: Experimental pressure distribution for the 7mm, -2 deg SS compared to EllipSys2D calculations α=4°.

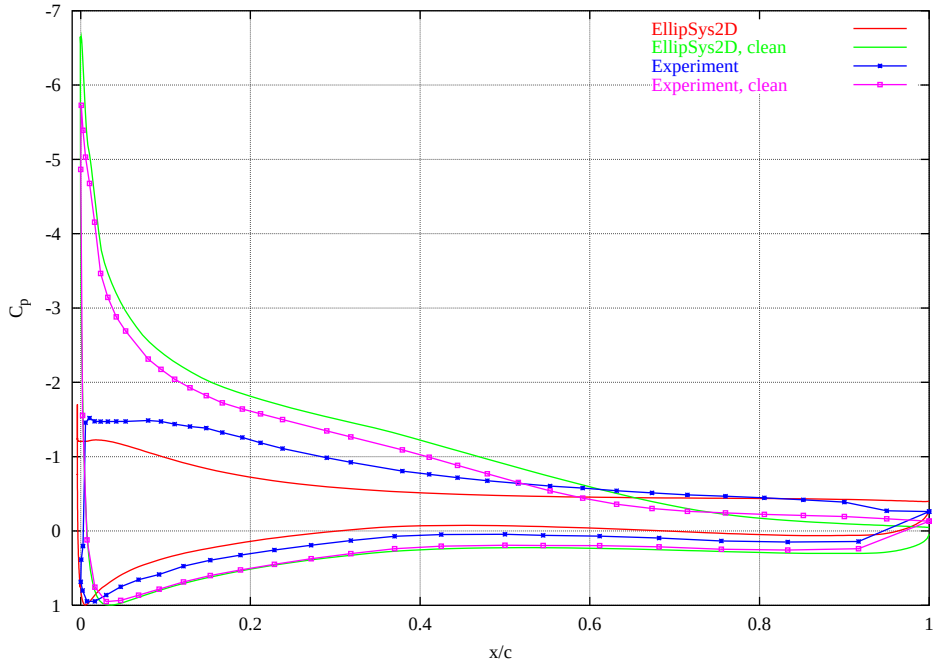

Figure 27: Experimental pressure distribution for the 7mm, -2 deg SS compared to EllipSys2D calculations α=12°.

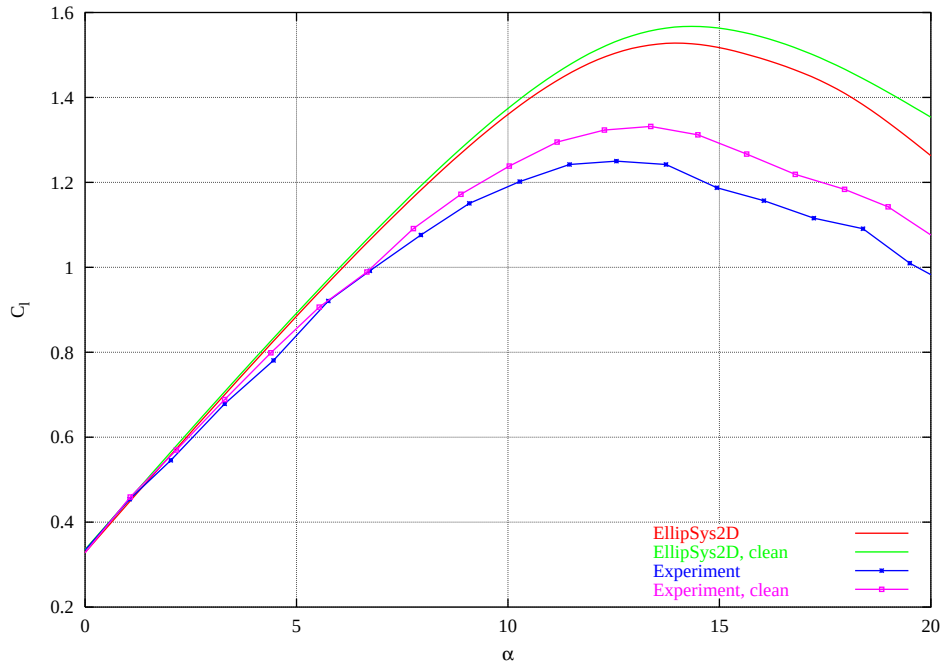

Figure 28: Experimental lift curve for the 5mm, 6 deg SS compared to Ellip-Sys2D calculations.

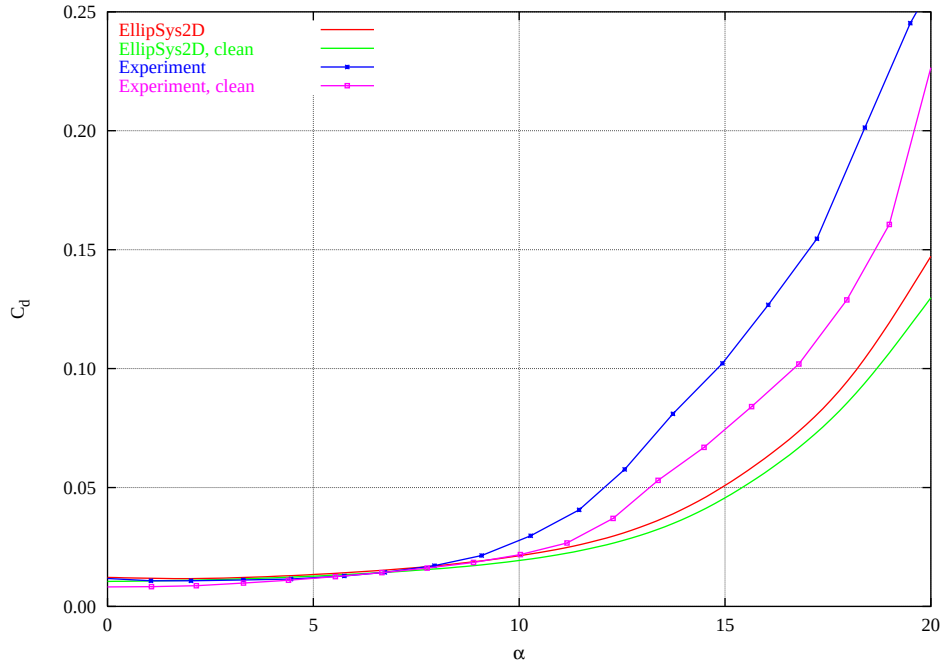

Figure 29: Experimental drag curve for the 5mm, 6 deg SS compared to Ellip-Sys2D calculations.

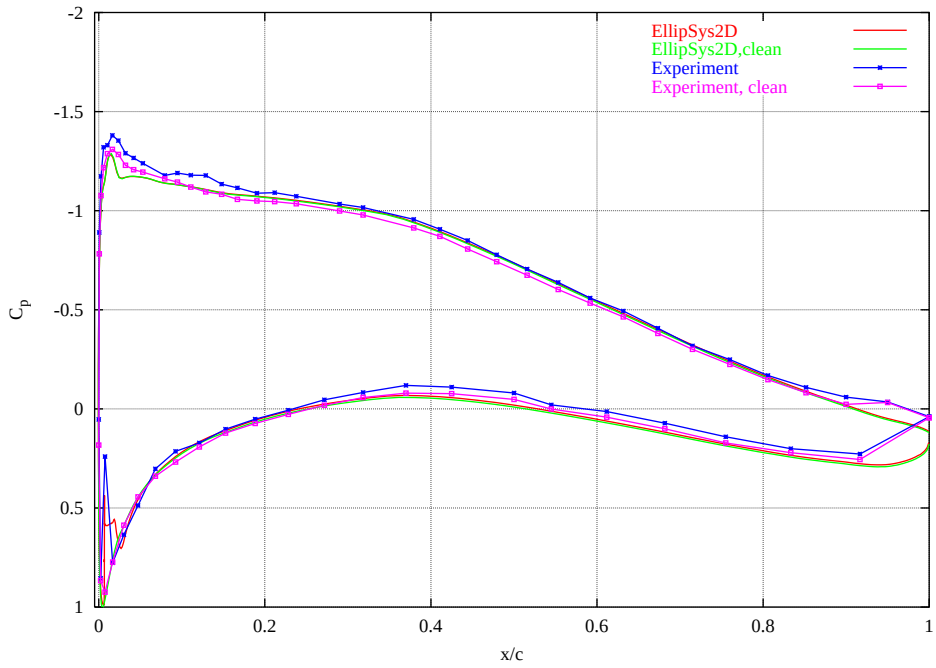

Figure 30: Experimental pressure distribution for the 5mm, 6 deg SS compared to EllipSys2D calculations α=4°.

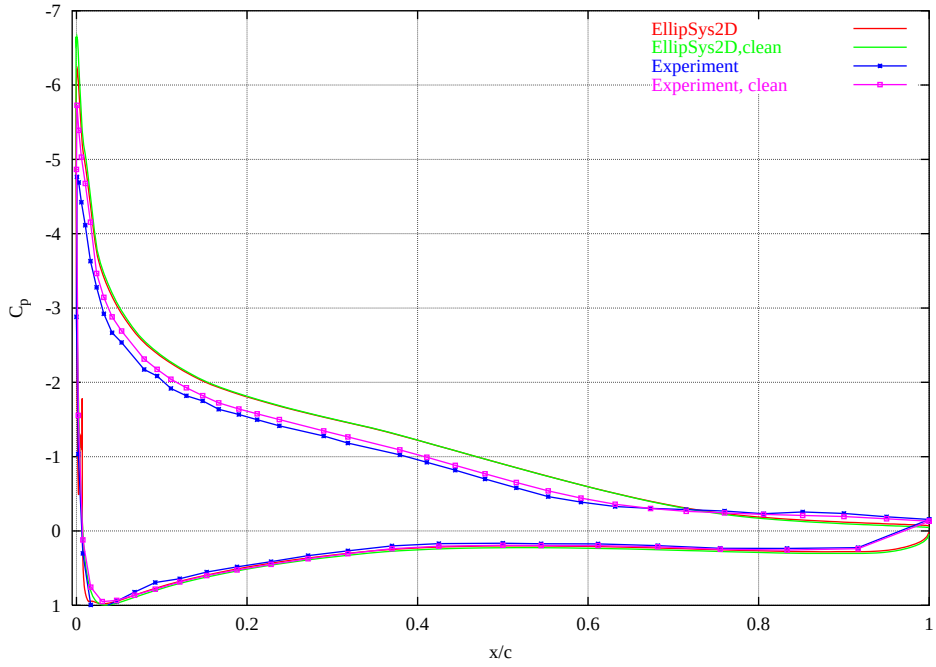

Figure 31: Experimental pressure distribution for the 5mm, 6 deg SS compared to EllipSys2D calculations α=12°.

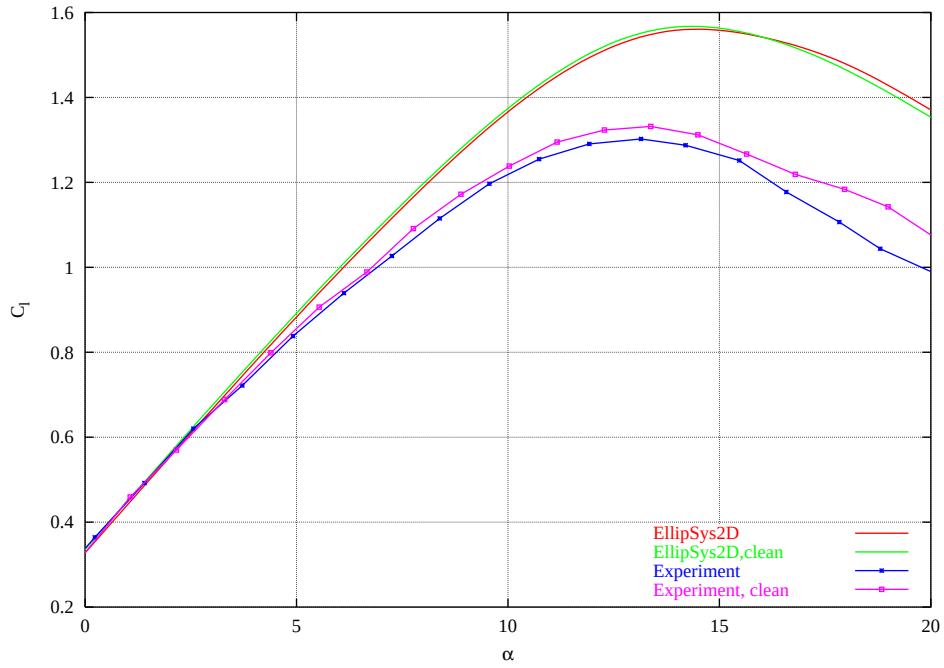

Figure 32: Experimental lift curve for the 5mm, 10 deg SS compared to Ellip-Sys2D calculations.

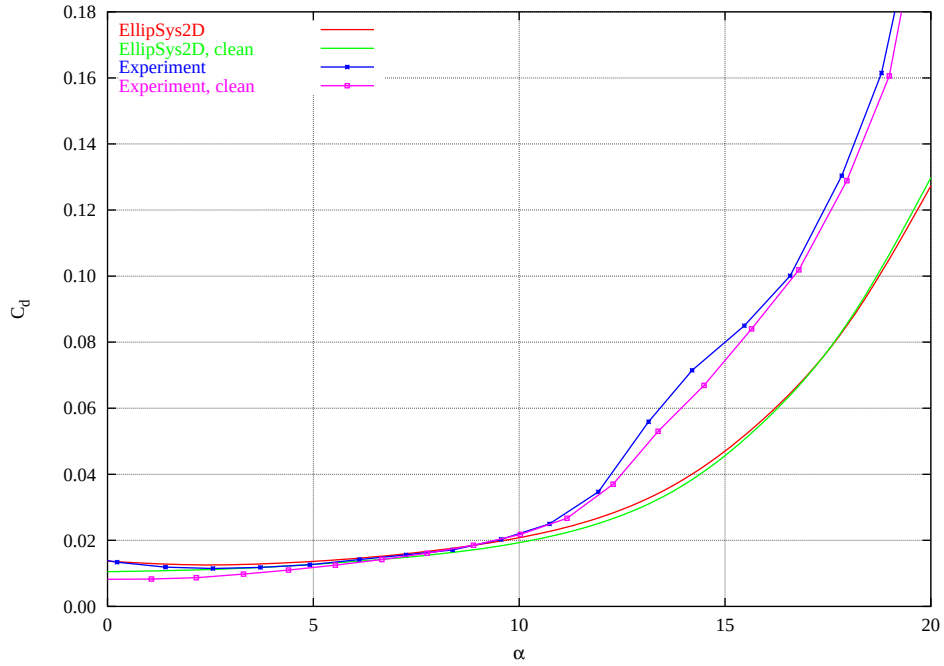

Figure 33: Experimental drag curve for the 5mm, 10 deg SS compared to Ellip-Sys2D calculations.

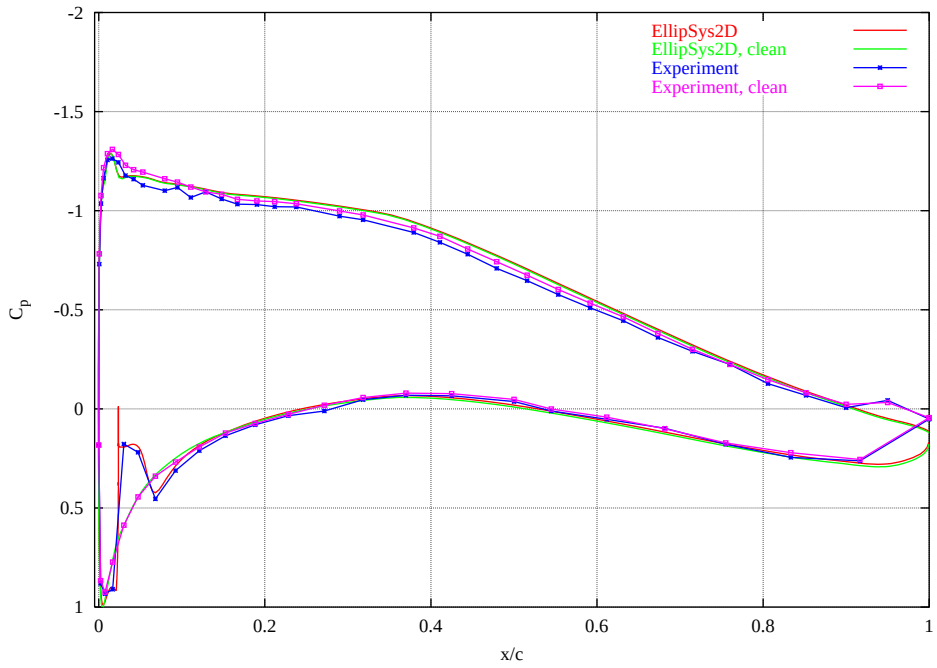

Figure 34: Experimental pressure distribution for the 5mm, 10 deg SS compared to EllipSys2D calculations α=4°.

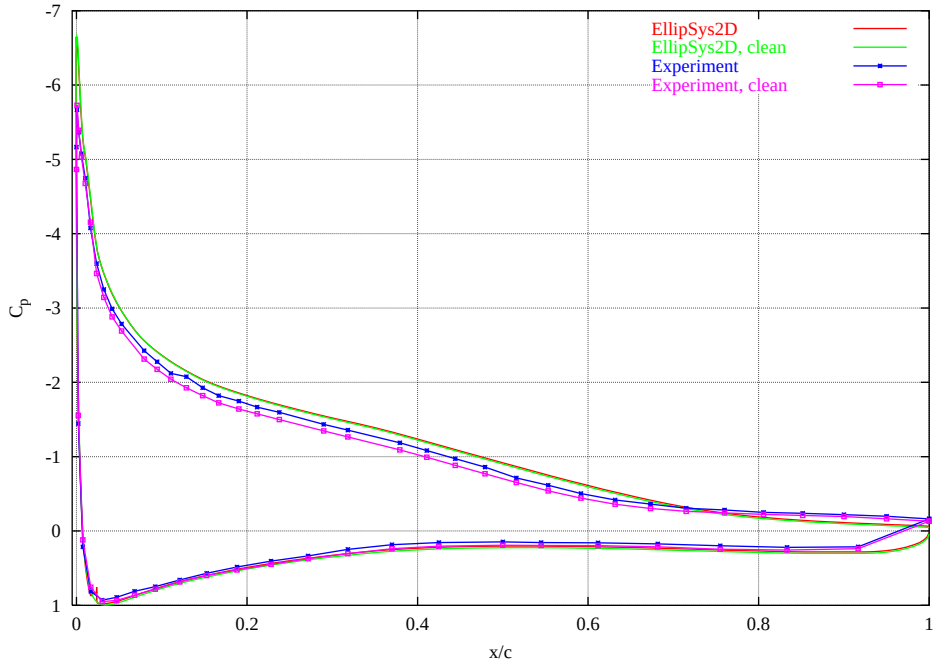

Figure 35: Experimental pressure distribution for the 5mm, 10 deg SS compared to EllipSys2D calculations α=12°.

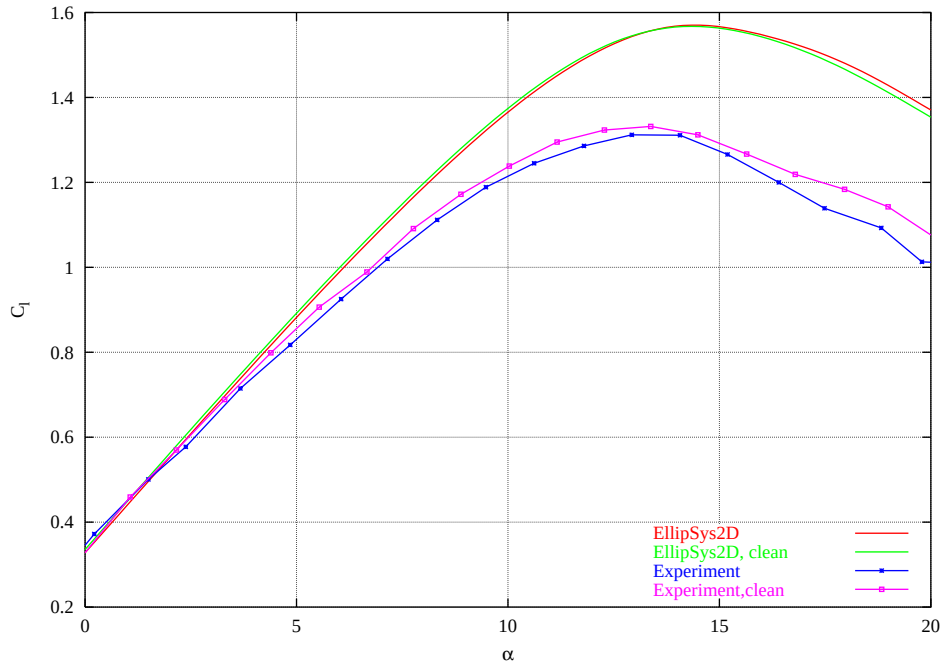

Figure 36: Experimental lift curve for the 5mm, 14 deg SS compared to EllipSys2D calculations.

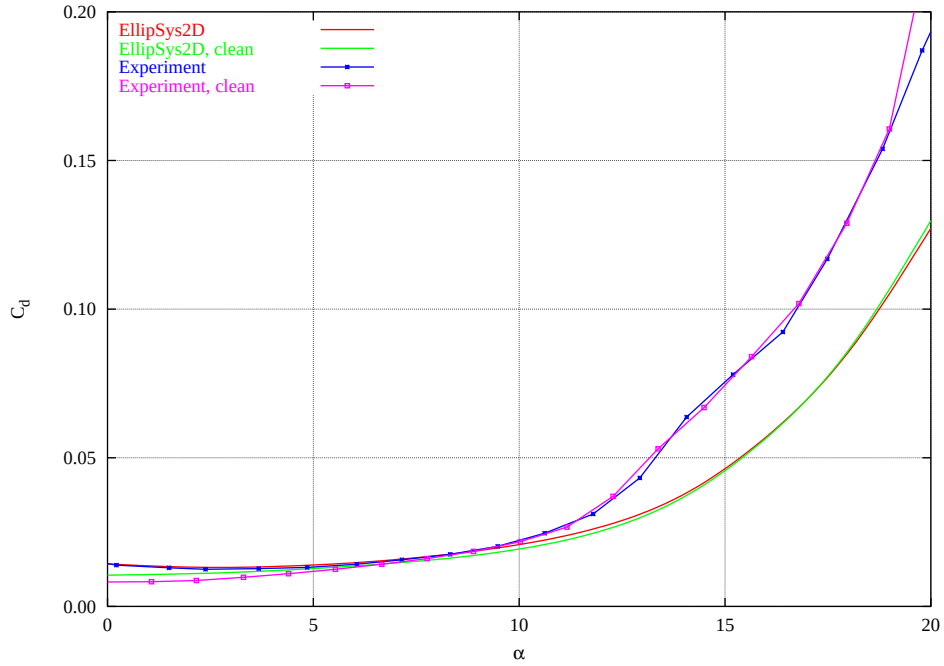

Figure 37: Experimental drag curve for the 5mm, 14 deg SS compared to EllipSys2D calculations.

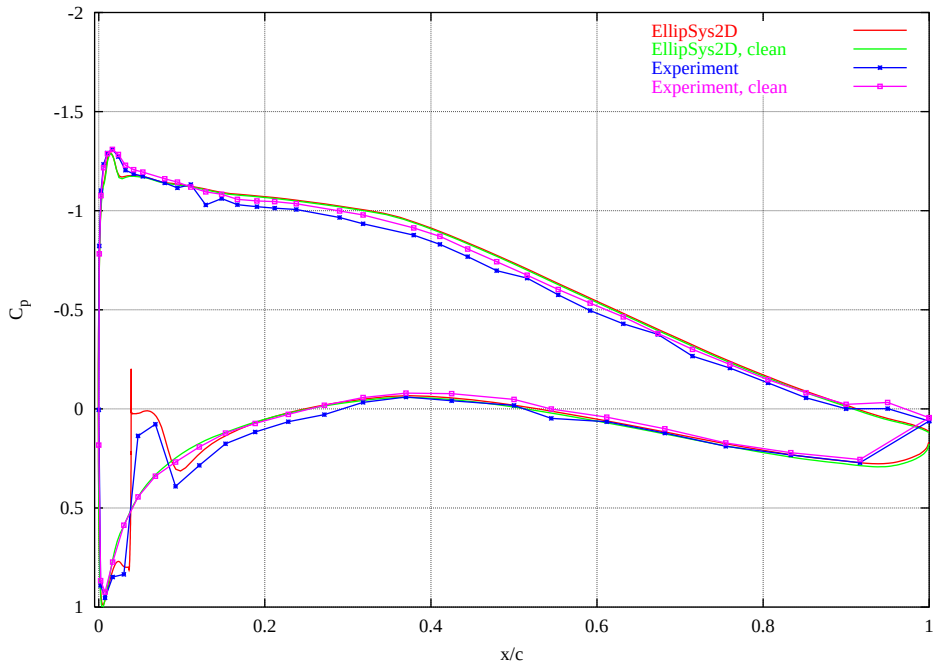

Figure 38: Experimental pressure distribution for the 5mm, 14 deg SS compared to EllipSys2D calculations α=4°.

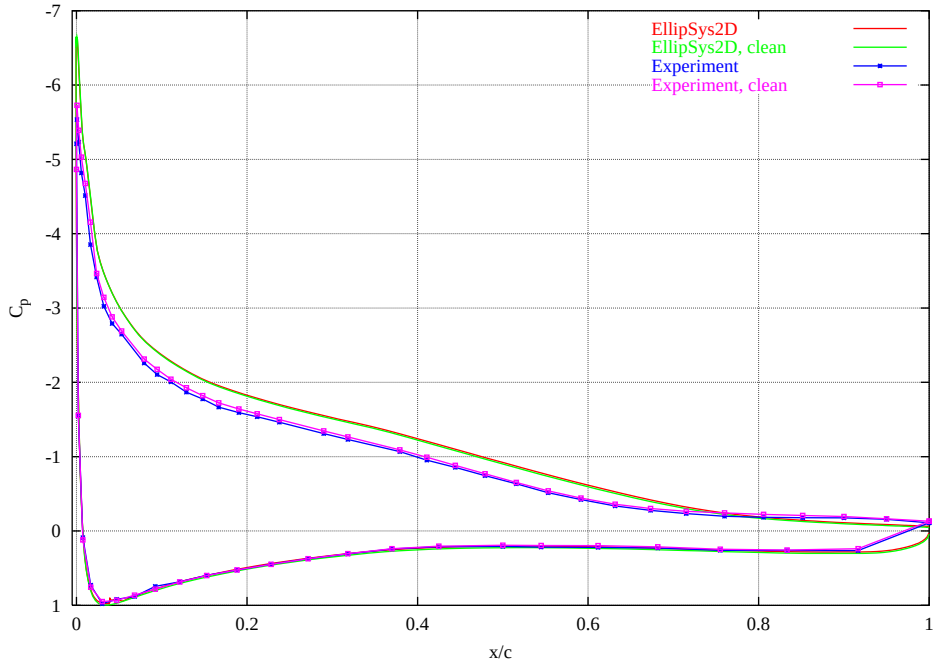

Figure 39: Experimental pressure distribution for the 5mm, 14 deg SS compared to EllipSys2D calculations α=12°.

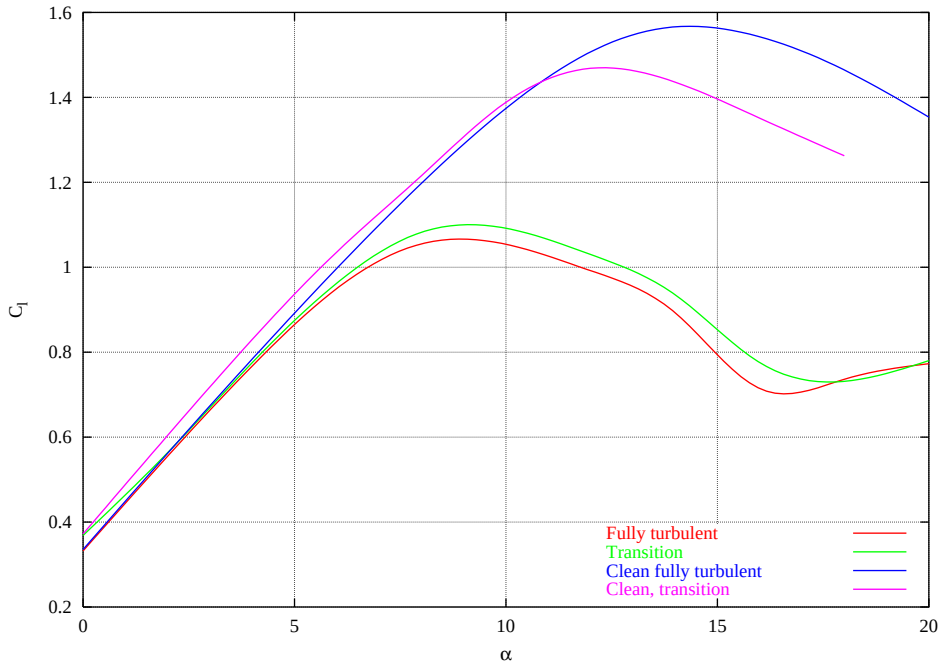

Figure 40: Comparison of the lift curves for the 7mm, 0 deg using fully turbulent computations and transitional computations.

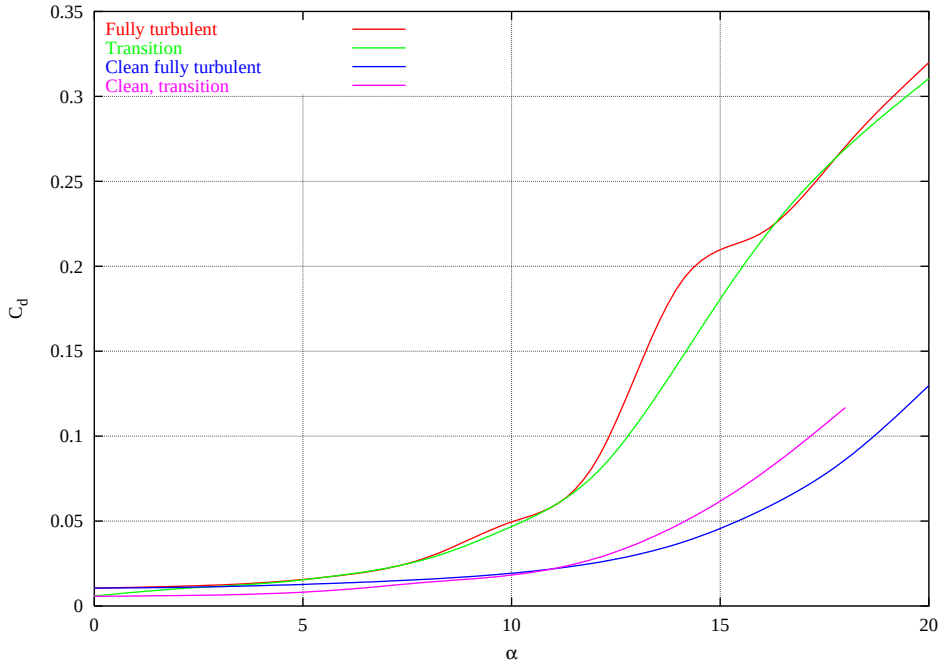

Figure 41: Comparison of the drag curves for the 7mm, 0 deg, using fully turbulent computations and transitional computations.

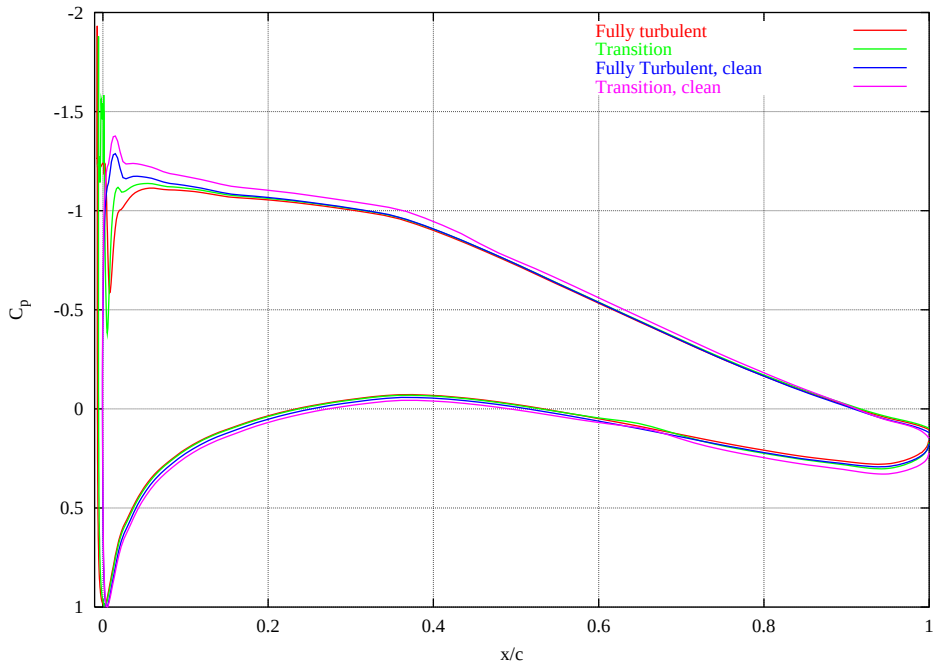

Figure 42: Comparison of the pressure distributions for the 7mm, 0 deg using fully turbulent computations and transitional computations, α=4°.

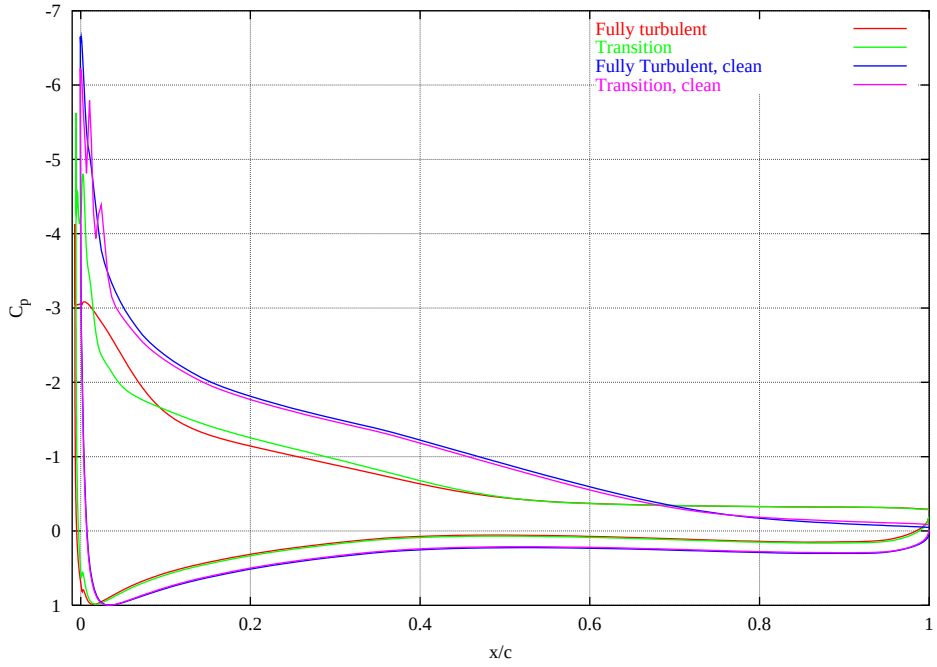

Figure 43: Comparison of the pressure distributions for the 7mm, 0 deg fully turbulent computations and transitional computations, α=12°.

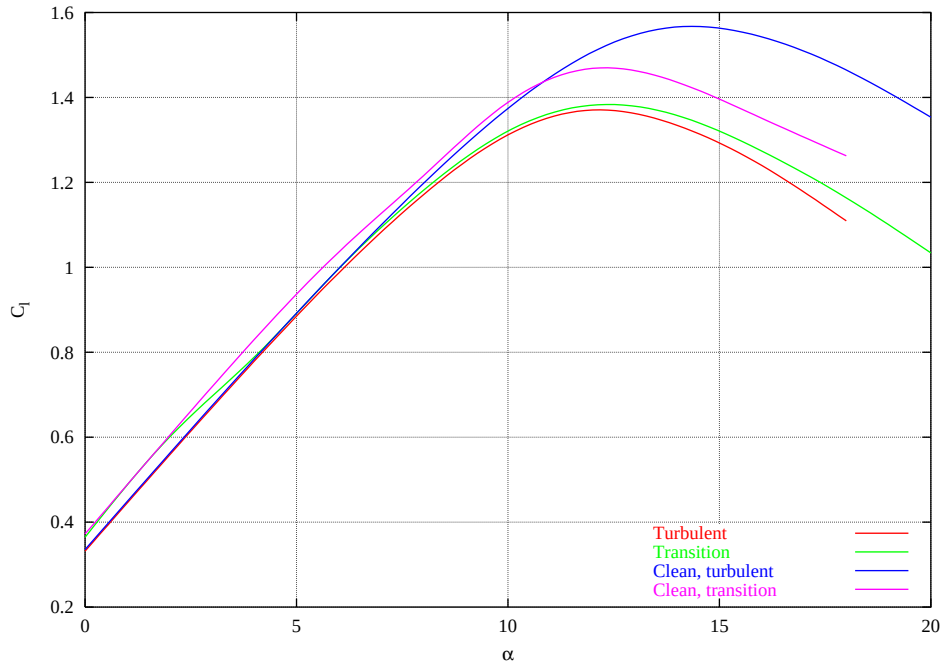

Figure 44: Comparison of the lift curves for the 7mm, 2 deg using fully turbulent computations and transitional computations.

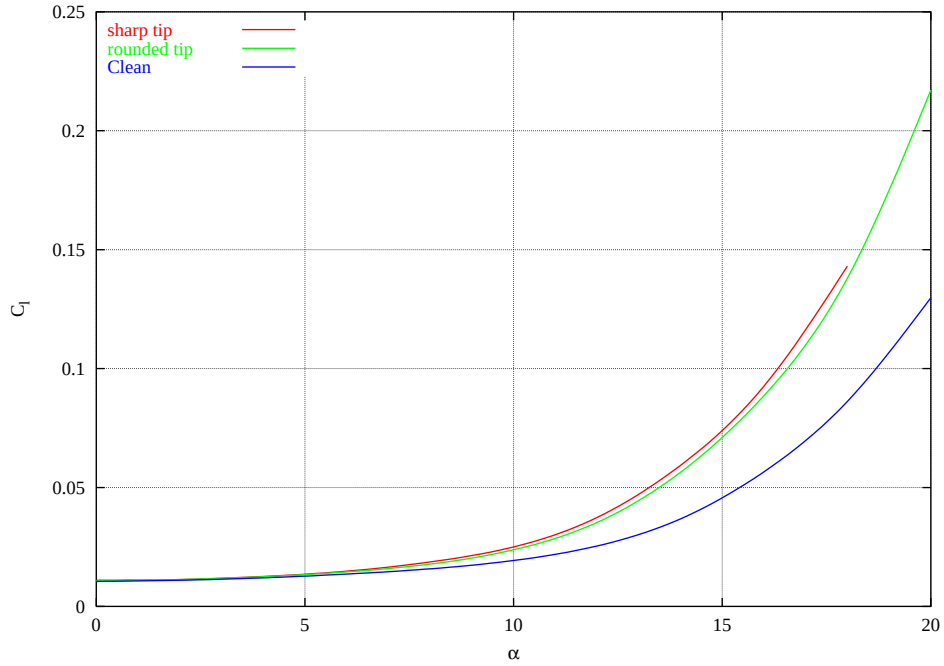

Figure 45: Comparison of the drag curves for the 7mm, 2 deg using fully turbulent computations and transitional computations.

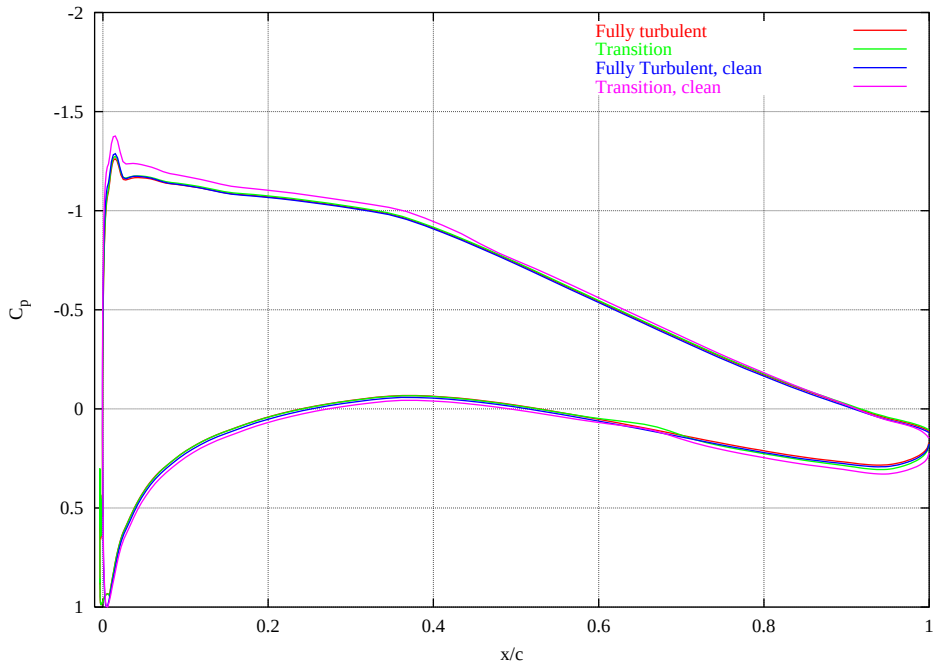

Figure 46: Comparison of the pressure distributions for the 7mm, 2 deg fully turbulent computations and transitional computations, α=4°.

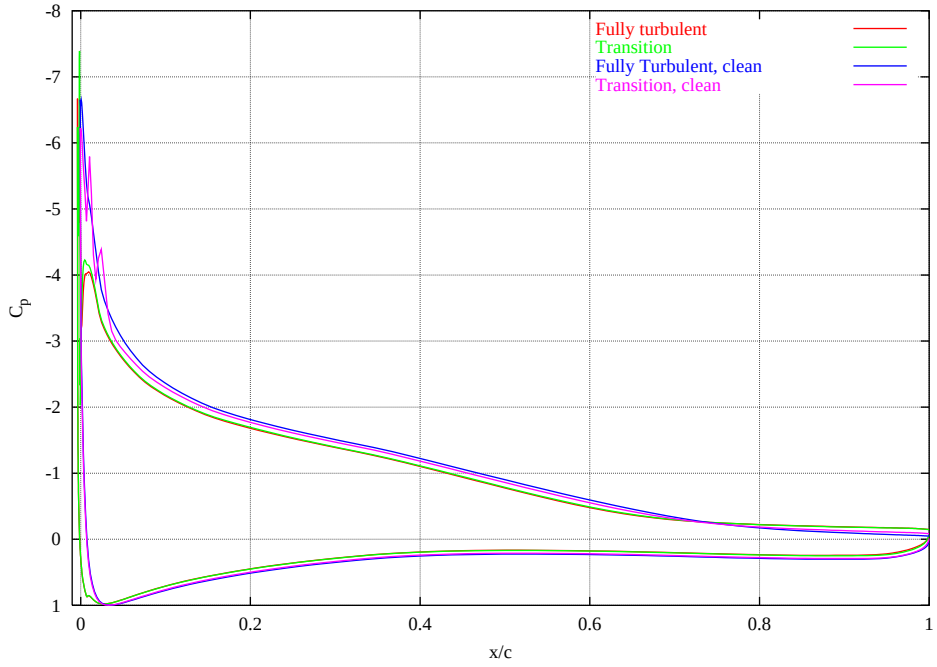

Figure 47: Comparison of the pressure distributions for the 7mm, 2 deg fully turbulent computations and transitional computations, α=12°.

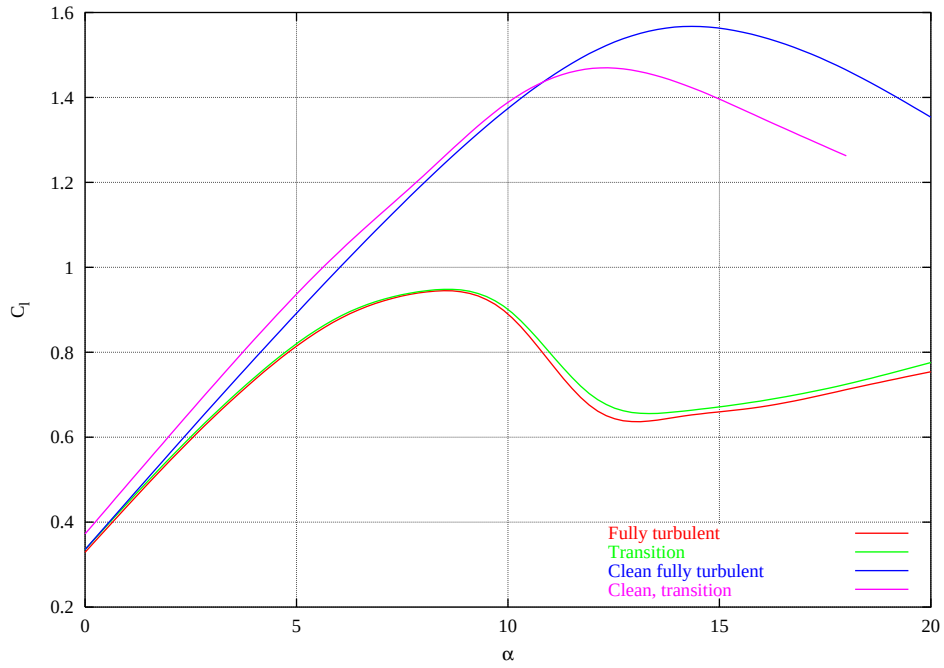

Figure 48: Comparison of the lift curves for the 7mm, -2 deg using fully turbulent computations and transitional computations.

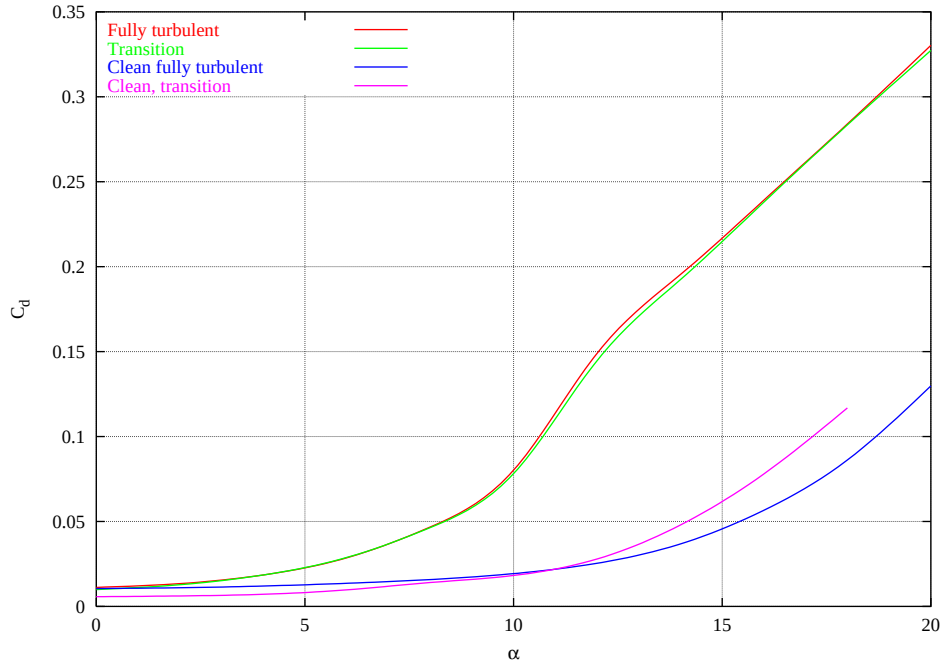

Figure 49: Comparison of the drag curves for the 7mm, -2 deg fully turbulent computations and transitional computations.

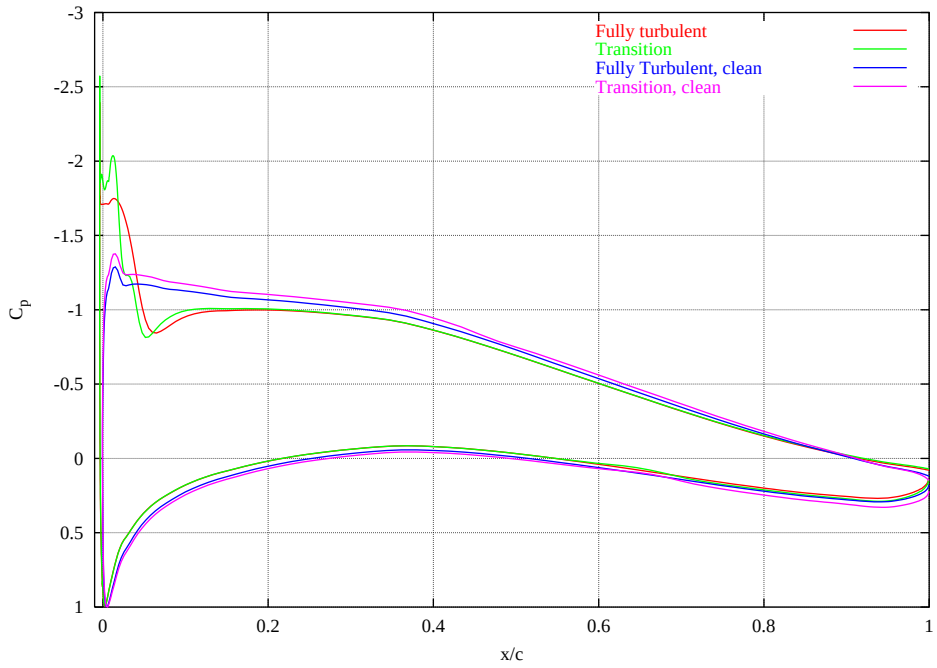

Figure 50: Comparison of the pressure distributions for the 7mm, -2 deg fully turbulent computations and transitional computations, α=4°.

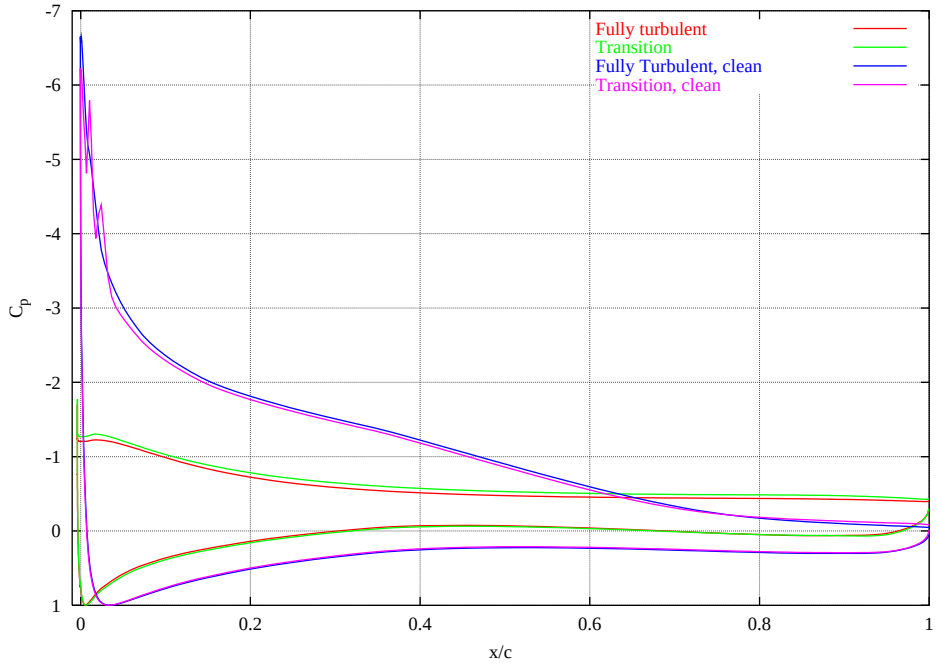

Figure 51: Comparison of the pressure distributions for the 7mm, -2 deg fully turbulent computations and transitional computations, α=12°.

6.2 Rounded Tip Stall Strips

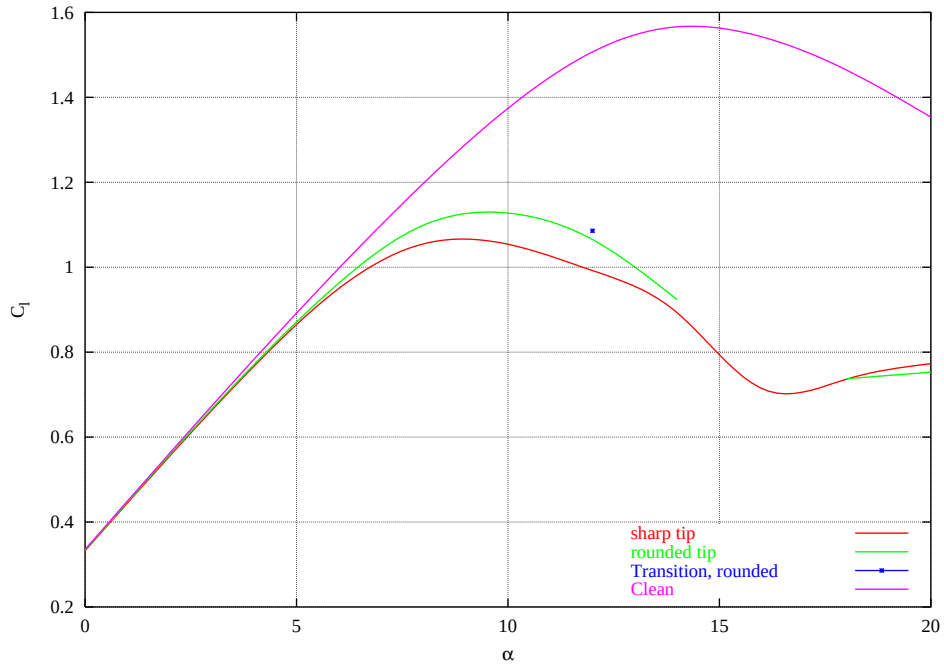

Figure 52: Comparison of the lift curves for the 7mm, 0 deg rounded tip SS and the sharp tip SS.

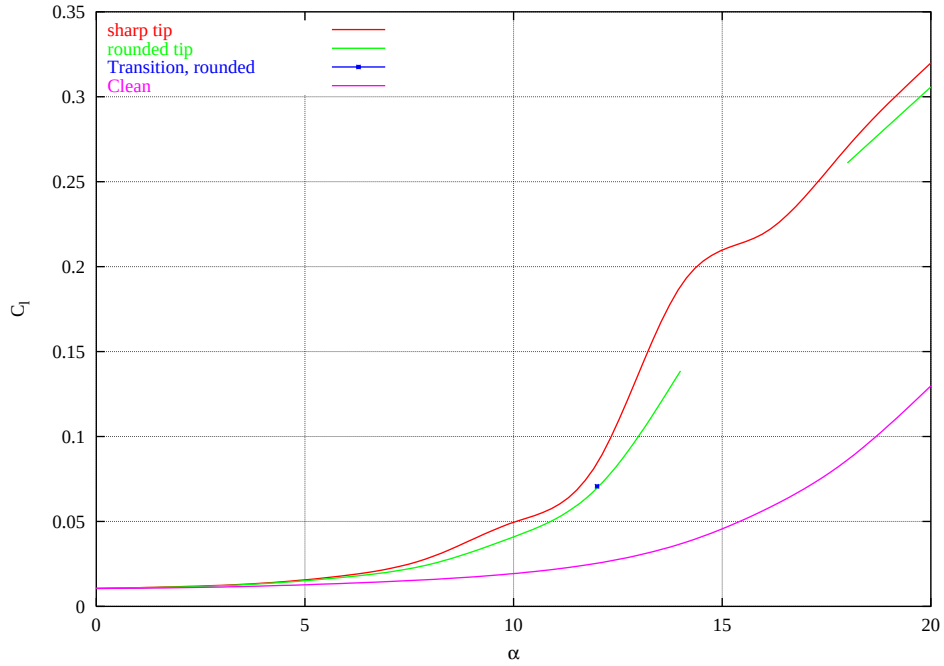

Figure 53: Comparison of the drag curves for the 7mm, 0 deg rounded tip SS and the sharp tip SS.

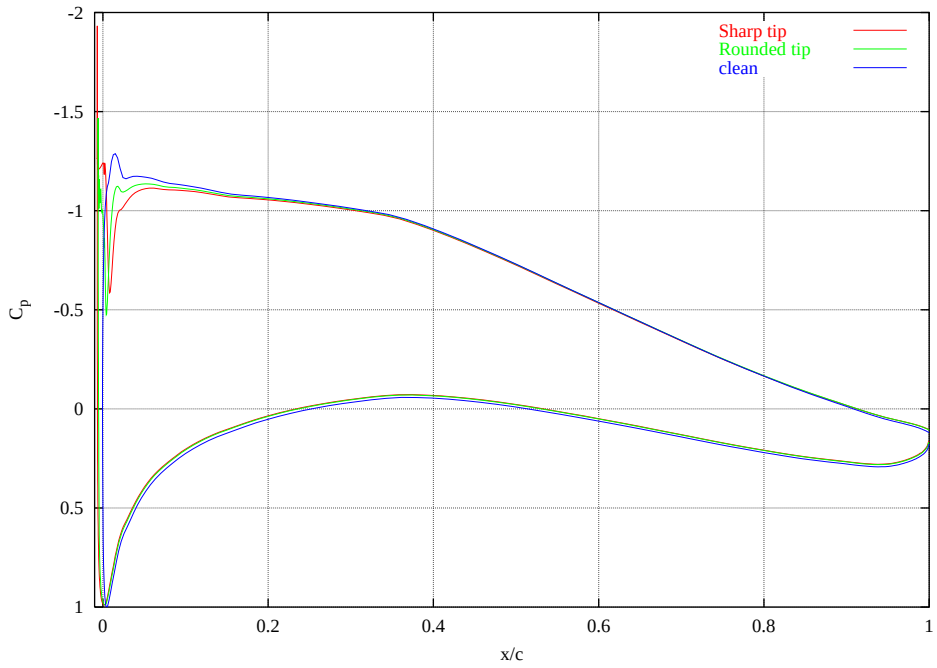

Figure 54: Comparison of the pressure distributions for the 7mm, 0 deg rounded tip SS and the sharp tip SS, α=4°.

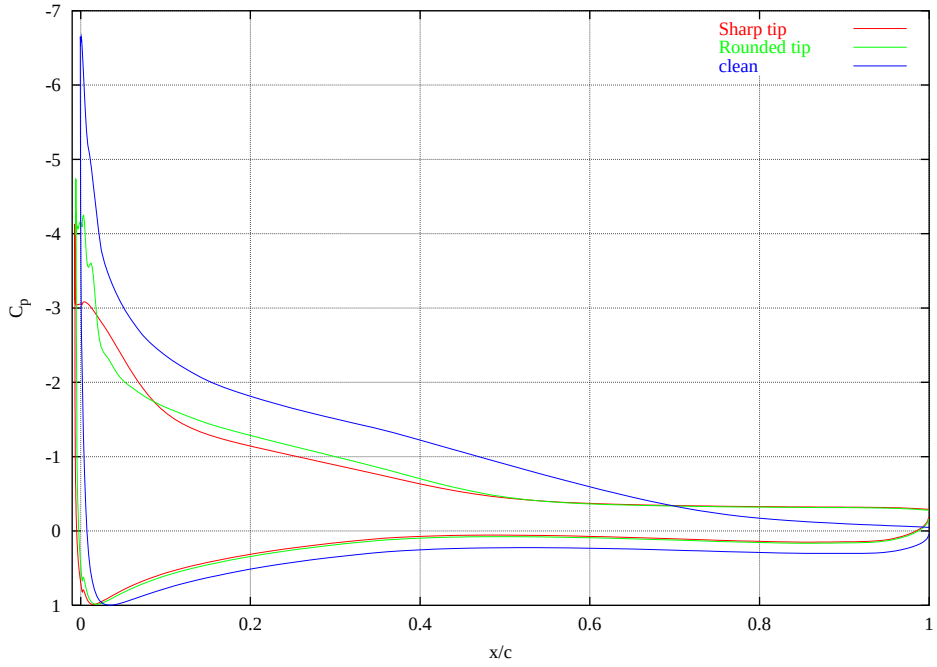

Figure 55: Comparison of the pressure distributions for the 7mm, 0 deg rounded tip SS and the sharp tip SS, α=12°.

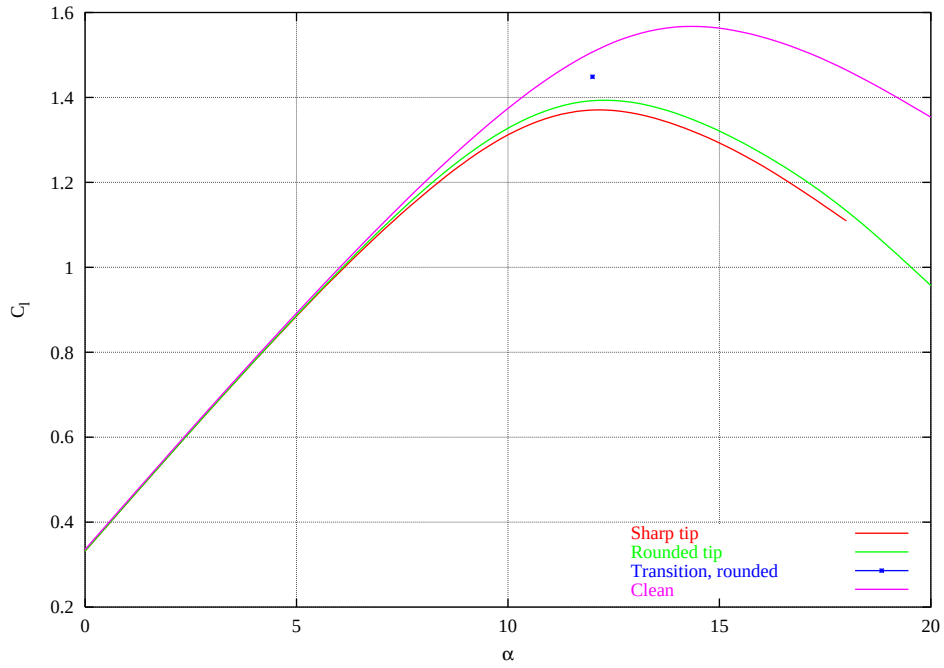

Figure 56: Comparison of the lift curves for the 7mm, 2 deg rounded tip SS and the sharp tip SS.

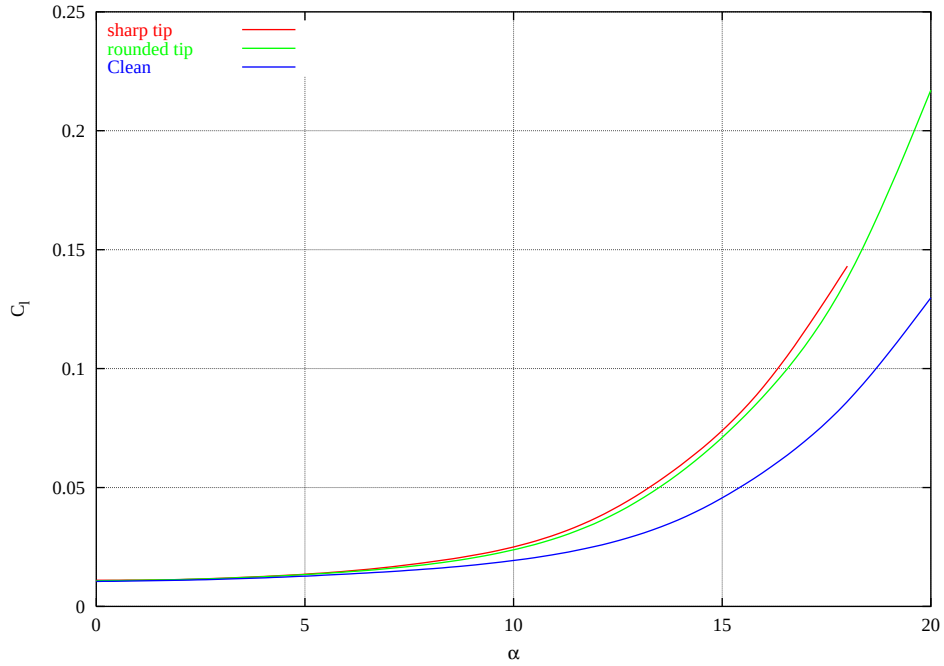

Figure 57: Comparison of the drag curves for the 7mm, 2 deg rounded tip SS and the sharp tip SS.

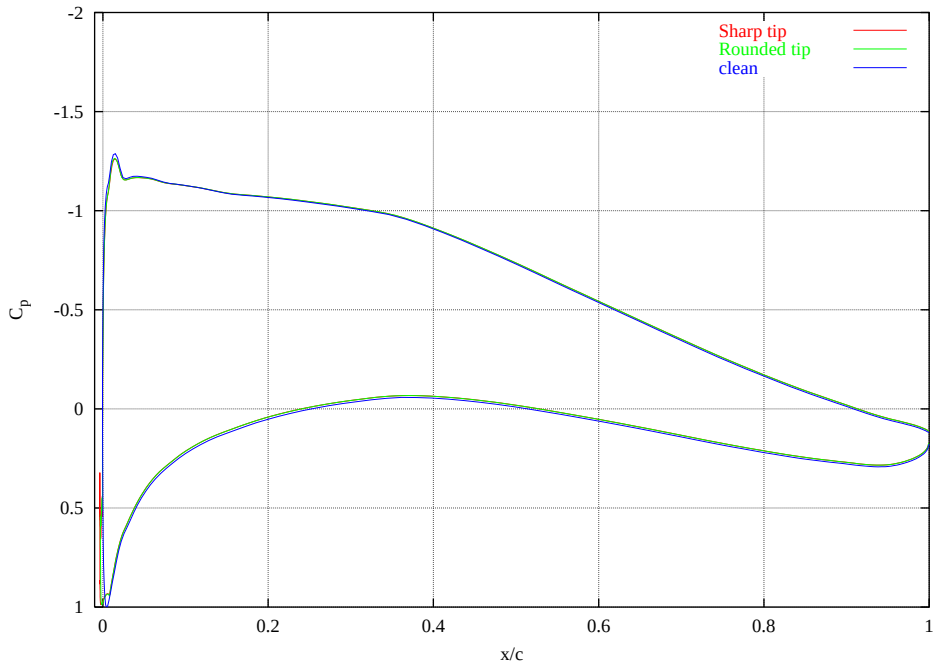

Figure 58: Comparison of the pressure distributions for the 7mm, 2 deg rounded tip SS and the sharp tip SS, α=4°.

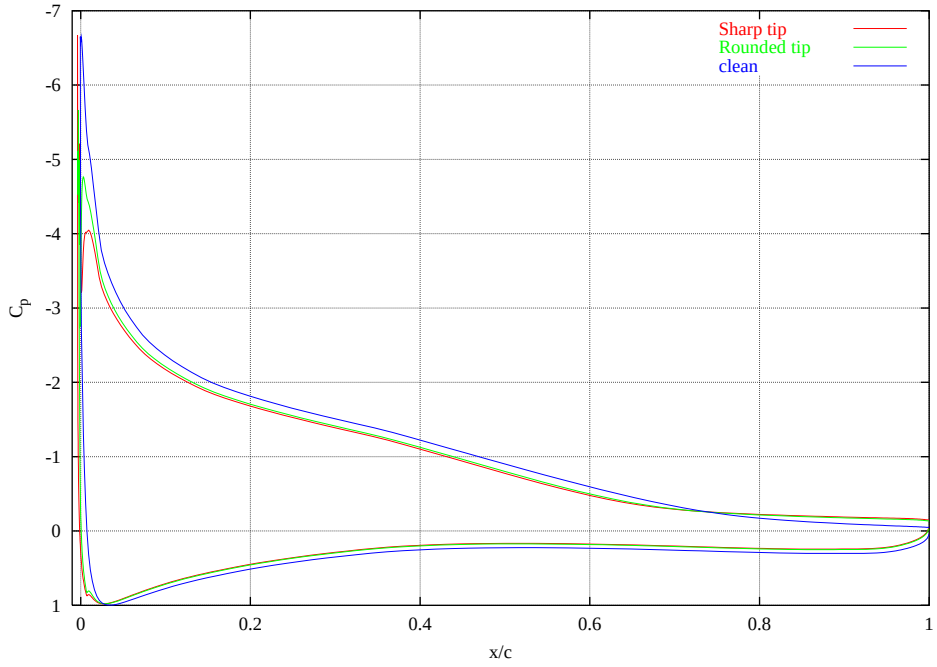

Figure 59: Comparison of the pressure distributions for the 7mm, 2 deg rounded tip SS and the sharp tip SS, α=12°.

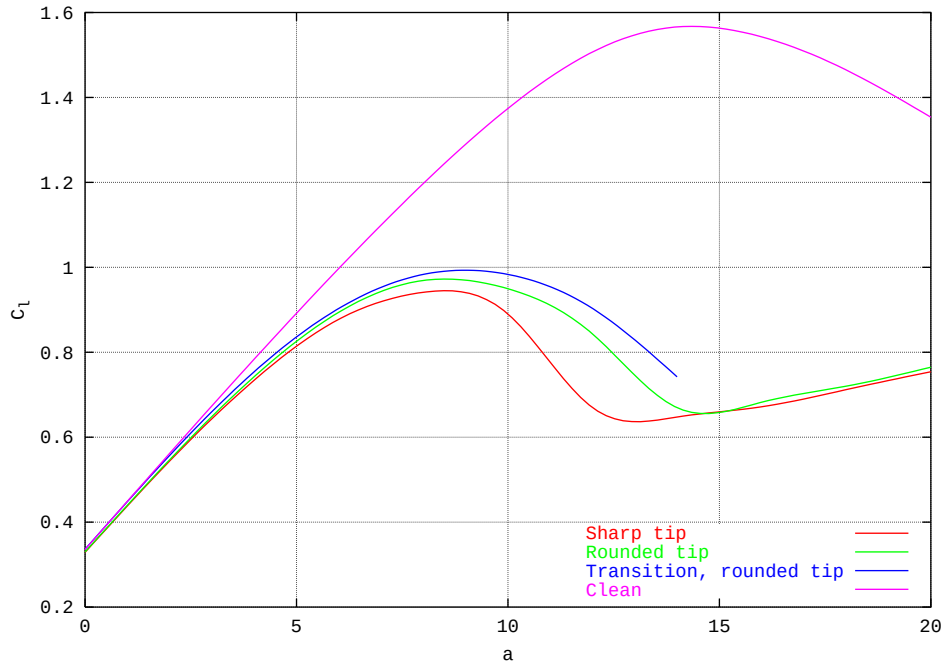

Figure 60: Comparison of the lift curves for the 7mm, -2 deg rounded tip SS and the sharp tip SS.

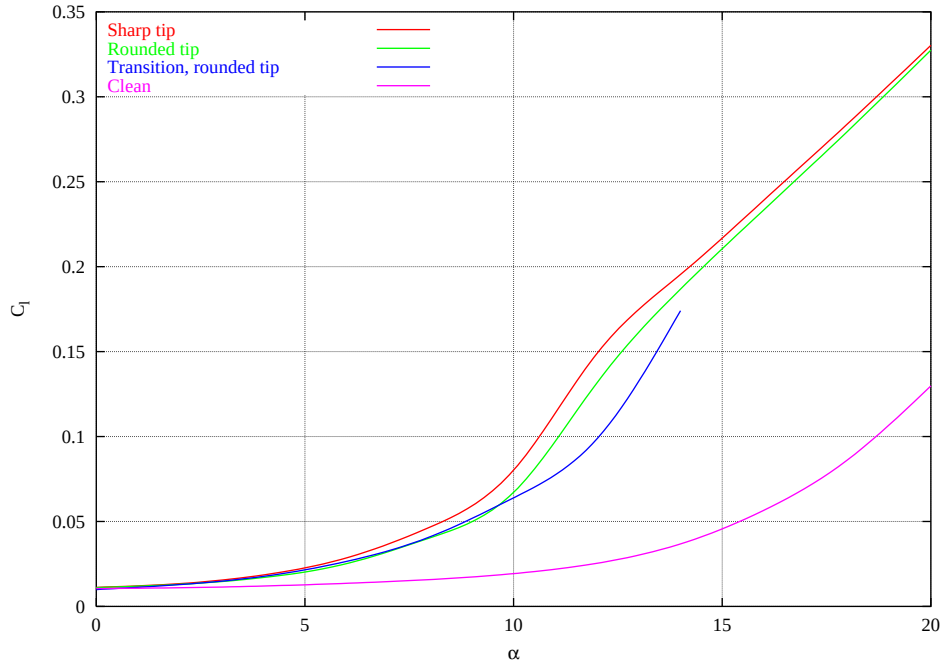

Figure 61: Comparison of the drag curves for the 7mm, -2 deg rounded tip SS and the sharp tip SS.

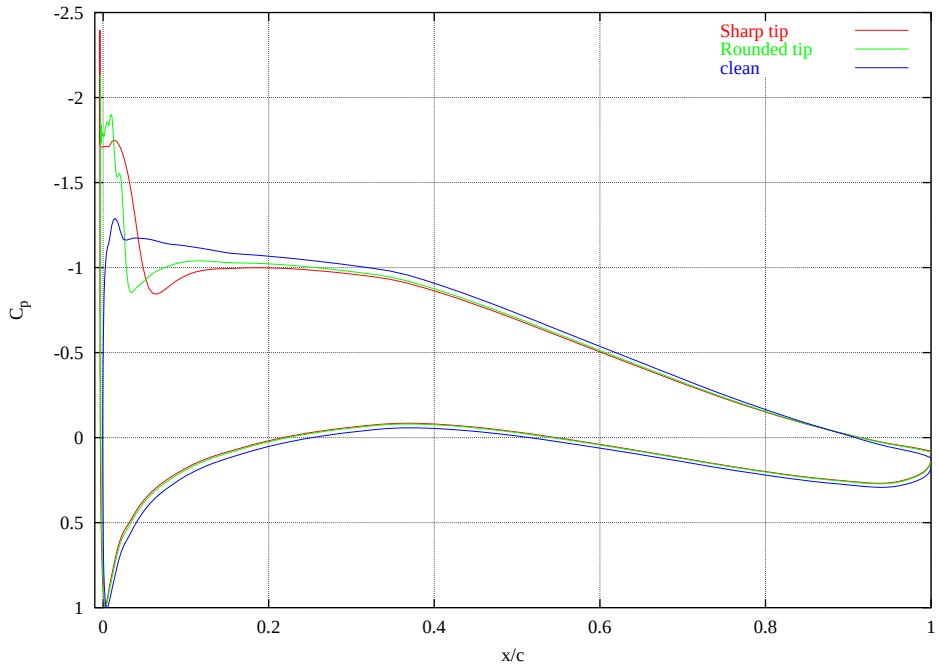

Figure 62: Comparison of the pressure distributions for the 7mm, -2 deg rounded tip SS and the sharp tip SS, α=4°.

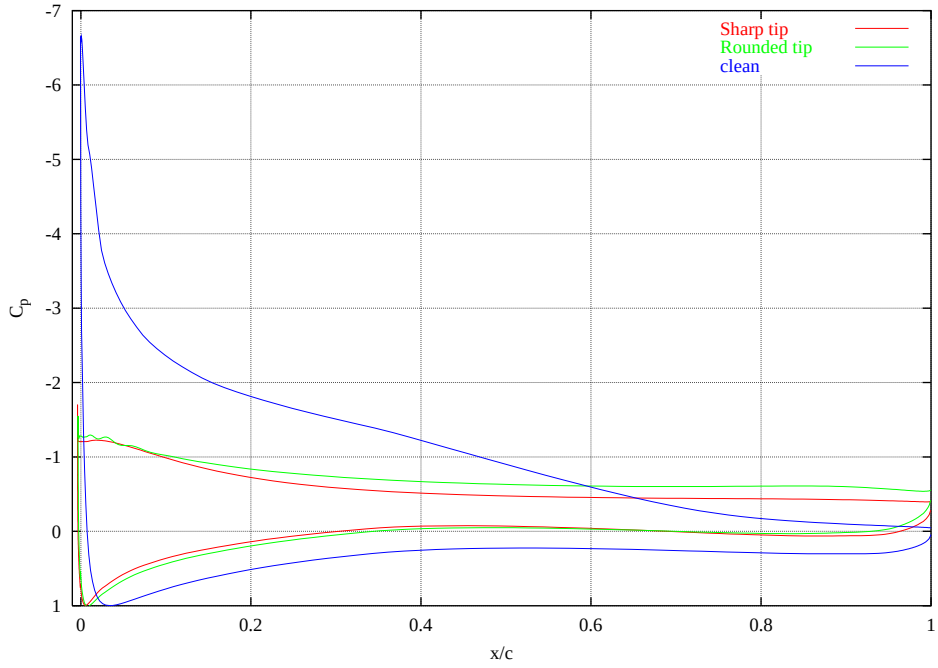

Figure 63: Comparison of the pressure distributions for the 7mm, -2 deg rounded tip SS and the sharp tip SS, α=12°.

Acknowledgements

The work was carried out under a contract wit EC, ENK-CT-2001-00503, KNOW-BLADE. Computations were made possible by the use of the IBM RS/6000 SP at the Risø central computing facility

References

1 Bak, C., Fuglsang, P., Johansen, J., Antoniou, I., 'Wind Tunnel Tests of the NACA 63-415 and a Modified NACA 63-415 Airfoil', Risø-R-1193(EN), Risø National Laboratory, Denmark (2000)

2 Sørensen, N. N., 'HypGrid, a 2D Mesh Generator', Risø-R-1035(EN), Risø National Laboratory, Denmark (1998).

3 Sørensen, N. N., 'Gereral Purpose Flow Solver Applied to Flow over Hills', Risø-R-827(EN), Risø National Laboratory, Denmark (1995).

4 Michelsen, J. A., 'Basis3D – A Platform for Development of Multiblock PDE Solvers', Tech. Report, Technical University of Denmark, AFM 92-05, 1992.

5 Michelsen, J. A., ' Block Structured Multigrid Solution of 2D and 3D Elliptic PDE's', Tech Report, Technical University of Denmark, AFM 94-06, 1994.

6 Bertagnolio, F., Johansen, J., Sørensen, N. N., 'Status for the Two-Dimensional Navier-Stokes Solver EllipSys2D', Risø-R-1282(EN), Risø National Laboratory, Denmark (2001).

7 Antoniou, I., Fuglsang, P., Madsen, H. Aa, Sørensen, N. N., 'Validation of a Wind Tunnel Testing Facility for Blade Surface Pressure Measurements', Risø-R-981(EN), Risø National Laboratory, Denmark (1998).

8 Abbot, I. H., Von Doenhoff, A. E., 'Theory of Wing Sections', Dover publications Inc, New York (1959).

9 Bertagnolio, F., Fuglsang, P., Johansen, J., Sørensen, N. N., 'Wind Turbine Airfoil Catalogue', Risø-R-1280(EN), Risø National Laboratory, Denmark (2001).

Appendix 1

Input files for mesh A2

gcf.dat:

```
********* General commands*************
1        : meshtype 1=cmesh, 2=omesh, 3=hmesh
384  128   : ni,nj         :number of cells in ksi, and eta
285       : Number of cells in boundary layer (nrbl)
14.d0    : domain_height :approximate hight of domain
1.d-5    : cell_height   :approximate hight of first cell
-1.d0      : Approximate height of boundary layer (bl_height)
-1.d0      : Approximate cell height at top of boundary layer
(blcell)
1        : dist_func     :stretching function tanh=1, sinh=2
.true.   : lspline       :surface representation (.true.-> spline
or linear)
1.d-5    : vol_blend     :blending of volume and mean volume
[0:0.4]
1.0d0     : diss_fac      :numerical dissipation factor
0        : nsmooth       :number of smoothing sweeps
0.d-1    : alpha0        :smooth factor
********* C-mesh commands*************
64         : iwake         :cells in wake (c/h-mesh)
12.0d0    : wake_lenght   :approximate lenght of wake (c/h-mesh)
10.0d0    : flow_angle    :Intended flow angle
10.0d0    : wake_angle    :wake angle at trailing edge
********* O-mesh commands*************
64 64     : ioutu ioutl   :outlet part of boundary (o-mesh)
0.3d0    : wake_contract :Wake contraction (o-mesh)
```

high.dat

```
# 6
0.00 40.0
0.10 10.0
0.15  1.0
0.85   1.0
0.90 10.0
1.00 40.0
```

dist.inp

```
0.0 0.0001  1
0.49617 0.0005 135
1.0 0.0001 256
```

Input files for mesh M2

gcf.dat:

```
********* General commands*************
1        : meshtype 1=cmesh, 2=omesh, 3=hmesh
448  128   : ni,nj         :number of cells in ksi, and eta
285       : Number of cells in boundary layer (nrbl)
14.d0    : domain_height :approximate hight of domain
1.d-5    : cell_height   :approximate hight of first cell
-1.d0      : Approximate height of boundary layer (bl_height)
-1.d0      : Approximate cell height at top of boundary layer
(blcell)
1        : dist_func     :stretching function tanh=1, sinh=2
.true.   : lspline       :surface representation (.true.-> spline
or linear)
1.d-5    : vol_blend     :blending of volume and mean volume
[0:0.4]
1.0d0     : diss_fac      :numerical dissipation factor
0        : nsmooth       :number of smoothing sweeps
0.d-1    : alpha0        :smooth factor
********* C-mesh commands*************
```

```
0          : iwake         :cells in wake (c/h-mesh)
12.0d0    : wake_lenght   :approximate lenght of wake (c/h-mesh)
10.0d0    : flow_angle    :Intended flow angle
10.0d0    : wake_angle    :wake angle at trailing edge
********* O-mesh commands*************
64 64     : ioutu ioutl   :outlet part of boundary (o-mesh)
0.3d0    : wake_contract :Wake contraction (o-mesh)
```

geometry.dat for SS P00:

```
#SURFACE DESCRIPTION
#FACE1 7
#SEC1 65
[wake coordinates]
#SEC2
[sec1.dat]
#SEC3 2
[SScoord1.dat]
#SEC4 2
[SScoord2.dat]
#SEC5
[sec2.dat]
#SEC6
[sec3.dat]
#SEC7 65
[wake coordinates]
#DISTRIBUTION FUNCTIONS
#FACE1 7
#SEC1 -1 65
-1 0.0005
#SEC2 -1 149
0.0005 0.0003
#SEC3 -1 53
0.0003 0.00005
#SEC4 -1 53
0.00005 0.0003
#SEC5 -1 3
0.0003 0.0005
#SEC6 -1 131
0.0005 0.0005
#SEC7 -1 65
0.0005 -1
```

The files sec*.dat and SScoord*.dat are obtained from the program SScoord.exe.

Input files for rounded tip SS

dist.inp for the SS:

```
0.0 0.013 1
0.5 0.004 52
1.0 0.013 105
```

The same gcf.dat and geometry.dat files were used as above. The coordinates for the curved SS's are obtained from the program SScoordcurved.exe.

Appendix 2

Dimensionless Normal Distance y+
The dimensionless normal distance y+ is defined as follows:

$$\tau_w = ½\rho U_\infty^2 c C_f$$

$$U\tau = \sqrt{\frac{\tau_w}{\rho}}$$

$$y+ = \frac{lU\tau}{\nu} = \frac{\rho l U\tau}{\mu}$$

Bibliographic Data Sheet **Risø-R-1370(EN)**

Title and authors

CFD Study of a NACA 63-415 Aerofoil Fitted with Stall Strips

Frederik Zahle, Niels N. Sørensen, Jeppe Johansen

ISBN	ISSN
87-550-3126-9 87-550-3127-7 (Internet)	0106-2840

Department or group	Date
Wind Energy Department	September 2002

Groups own reg. number(s)	Project/contract No(s)
	ENK6-CT-2001-00503

Pages	Tables	Illustrations	References
51	8	63	9

Abstract (max. 2000 characters)

Abstract The present work describes a thorough investigation of 2D computations of the flow around a NACA 63-415 aerofoil fitted with stall strips (SS). A mesh study as well as a time step study is carried out and all computations are compared with experiments. Two different SS, 5mm and 7mm are investigated at several positions. Furthermore the influence of laminar to turbulent transition and the effect of a rounded SS were tested.

There is not sufficient agreement between the experimental results and the simulations to draw any conclusions of optimum position and geometry of the SS. The 7mm SS's placed at P00 and P-02 has the greatest effect on the max lift followed by SS P02. The 5mm SS's does, as in the experiment, not change the lift curve noticeably. Even though this investigation does not conclusively succeed in verifying the experimental results with CFD, many useful conclusions can be drawn from the results.

It is observed in the experiment that the vertical force fluctuates at higher angles of attack. This indicates that small bubbles are being shed off the profile causing the force to vary. This property is observed when transition is included in the model and also when the tip of the SS is rounded. From this result it could be concluded that the level of turbulence produced on the tip of the SS is very important for the development of the flow downstream. In the sharp tip calculations using fully turbulent computations, this is most likely too high, which resulted in the fine structures being damped out, with only one bubble appearing.

Descriptors INIS/EDB

AERODYNAMICS, COMPUTATIONAL FLUID DYNAMICS, NAVIER-STOKES EQUATIONS, STALL STRIPS, WIND TURBINES